Organic Geochemistry 108 (2017) 61–81

Contents lists available at ScienceDirect

Organic Geochemistry

journal homepage: www.elsevier.com/locate/orggeochem

Discovery of oil bitumen co-existing with solid bitumen in the Lower Cambrian Longwangmiao giant gas reservoir, Sichuan Basin, southwestern China: Implications for hydrocarbon accumulation process

Chunhua Shi [a,b], Jian Cao [a,*], Xiucheng Tan [c,d,e], Bing Luo [f], Wei Zeng [c,d,e], Wenxuan Hu [a]

[a] State Key Laboratory for Mineral Deposits Research, Department of Earth Sciences, Nanjing University, Nanjing 210023, China
[b] State Key Laboratory of Oil and Gas Reservoir Geology and Exploitation, Chengdu University of Technology, Chengdu, Sichuan 610059, China
[c] State Key Laboratory of Oil and Gas Reservoir Geology and Exploitation, Southwest Petroleum University, Chengdu 610500, China
[d] Division of Sedimentology and Hydrocarbon Accumulation, PetroChina Key Laboratory of Carbonate Reservoir, Southwest Petroleum University, Chengdu 610500, China
[e] School of Earth Science and Technology, Southwest Petroleum University, Chengdu 610500, China
[f] Research Institute of Exploration and Development, PetroChina Southwest Oil and Gas Field Company, Chengdu, Sichuan 610051, China

ARTICLE INFO

Article history:
Received 16 August 2016
Received in revised form 7 March 2017
Accepted 8 March 2017
Available online 3 April 2017

Keywords:
Reservoir bitumen
High maturity
Source–hydrocarbon correlation
Natural gas
Neoproterozoic Sinian Dengying formation

ABSTRACT

Natural gas in the recently discovered Lower Cambrian Longwangmiao giant gas reservoir of the Sichuan Basin in southwestern China has been considered to be from oil-cracking and sourced from the underlying Lower Cambrian Qiongzhusi shales, similar to the underlying Neoproterozoic Dengying giant gas reservoir. However, geological considerations and differences in geochemistry between the Longwangmiao and Dengying gases/bitumens imply different scenarios. Organic petrology, geochemistry and trace element analyses of widely occurring bitumen were conducted to evaluate this hypothesis. Results show the coexistence of solid bitumen and oil bitumen in this reservoir for the first time, which implies a new hydrocarbon accumulation process and associated exploration strategies. The two types of bitumen were termed Type A solid bitumen and Type B oil bitumen, which were sourced from the Lower Cambrian Qiongzhusi Formation shale and the Lower Silurian Longmaxi shale, respectively. The Type A solid bitumen shows little fluorescence and its color under plane-polarized light is almost black. This indicates that the Type A solid bitumen is likely of high maturity. It typically occurs in dissolution pores, and accounts for approximately 90% of all bitumen in the reservoir. In contrast, the Type B oil bitumen is brown–black in color under plane-polarized light, and yellow–green under fluorescence light, indicating that it is mature. It occurs in the residual spaces of the solid bitumen, and represents approximately 10% of the total bitumen content. This suggests that Type A bitumen charged the reservoir earlier than did the Type B bitumen. During the Indosinian Epoch of the Triassic, oil generated from the mature Qiongzhusi Formation migrated into the Longwangmiao and Dengying reservoirs. Following this, the Dengying reservoir reached the temperature threshold for oil cracking since the Late Cretaceous, and it is suggested that oil could have started to crack to gas, which is the critical moment for the gas formation. However, the Longwangmiao oils had not been cracked at this stage because the reservoir temperature had not reached the threshold. Later, during the Himalayan Epoch, the gas in the Dengying reservoir, as well as some kerogen-cracking gas from the Qiongzhusi shales, migrated into the Longwangmiao reservoir along faults. Gas gravity drainage and phase separation took place in the Longwangmiao reservoir, forming the Type A solid bitumen and giant gas accumulation. Later, oil generated from the Longmaxi shales migrated into the Longwangmiao reservoir, forming the Type B oil bitumen. The case here is an example of a multi-stage oil and gas accumulation. Future exploration targets should include Middle–Upper Cambrian reservoir rocks.

1. Introduction

Cambrian (including underlying Neoproterozoic and Mesoproterozoic) reservoir rocks (conventional oil and gas) and source rocks (unconventional shale oil and gas) have traditionally not been

* Corresponding author. Fax: +86 25 83686016.
E-mail address: jcao@nju.edu.cn (J. Cao).

http://dx.doi.org/10.1016/j.orggeochem.2017.03.004
0146-6380/

considered viable commercial oil and natural gas exploration targets due to their long and complex geological history and great burial depth, and thus only account for < 1% of discovered petroleum resources (Klemme and Ulmishek, 1991; Wang and Han, 2011). However, with the depletion of hydrocarbon reserves hosted in shallower rocks, Cambrian–Proterozoic units are increasingly being explored for their petroleum potential, resulting in significant discoveries, such as the Khazzan gas field in Oman (Rylance et al., 2011), the Amadeus Basin in Australia (natural gas; Edgoose, 2012; Swanson-Hysell et al., 2012), and the Tarim (oil and natural gas) and Sichuan basins (natural gas) in China (Zhu et al., 2012; Zheng et al., 2013; Zou et al., 2014a). In addition, these reservoirs occur at the boundary between the Cambrian and the Proterozoic, indicating that they may be of particular general geological significance (Pedersen et al., 2007; Liang et al., 2009; Carminati et al., 2010; Du et al., 2012; Sahu et al., 2013; Zou et al., 2014a).

In 2012, a large (approximately 1 trillion m^3 of total gas in place) marine carbonate gas reservoir was discovered in the Lower

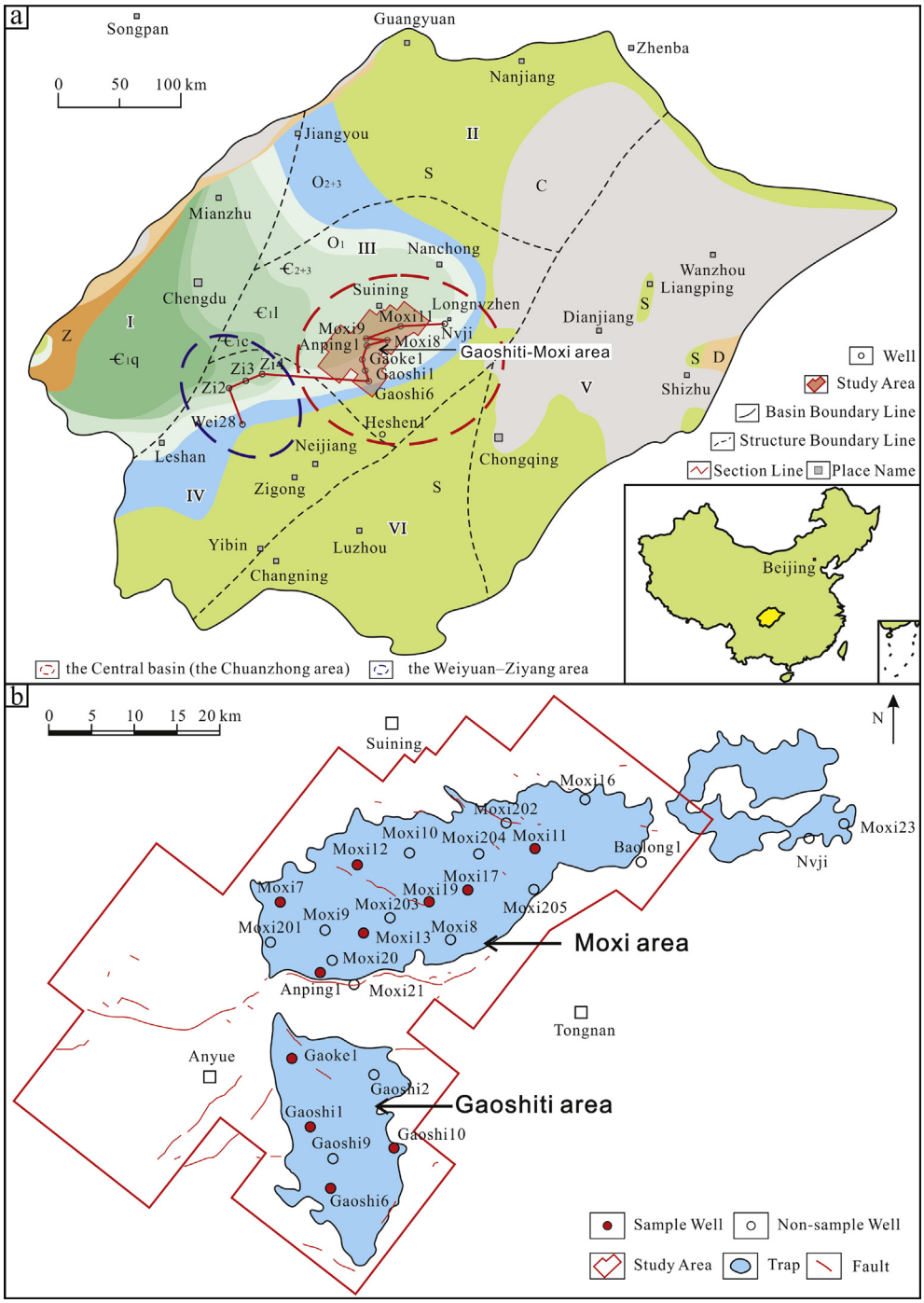

Fig. 1. Geological map showing: (a) pre-Permian sediments of the Sichuan Basin and the location of the study area, and (b) occurrence of the Longwangmiao Formation traps. I: Western Sichuan Depression; II: Northern Sichuan Low-lying and Flat Fold Belt; III: Central Sichuan Flat Fold Belt; IV: Southwestern Sichuan Low-lying and Sharp Fold Belt; V: Southeastern Sichuan High and Sharp Fold Belt; VI: Southern Sichuan Low-lying and Sharp Fold Belt. Z: Sinian; ϵ_1q: the Lower Cambrian Qiongzhusi Formation; ϵ_1c: the Lower Cambrian Canglangpu Formation; ϵ_1l: the Lower Cambrian Longwangmiao Formation; ϵ_{2+3}: the Middle and Upper Cambrian; O_1: the Lower Ordovician; O_{2+3}: the Middle and Upper Ordovician; S: Silurian; D: Devonian; C: Carboniferous.

Cambrian Longwangmiao Formation of the Moxi area, Leshan–Longnvsi paleo-uplift, Sichuan Basin, southwestern China (Figs. 1 and 2). This discovery, together with the discovery of the underlying Neoproterozoic Sinian Dengying giant gas reservoir in 2011 (Wei et al., 2014), has resulted in the study of several aspects of Cambrian–Neoproterozoic oil–gas formation and characteristics in this basin since 2012 (Yao et al., 2013; Li et al., 2014a, 2014b; Wei et al., 2014; Xu et al., 2014; Zheng et al., 2014). Thus, Li et al. (2014a) studied the evolution of the Caledonian paleo-uplift in the Sichuan Basin, and found that structures in the Gaoshiti–Moxi–Longnvsi Belt, and its northern extension, acted as structural traps in the Lower Paleozoic gas reservoir. In addition, they concluded that Cambrian and Upper Ordovician rocks provided the best karstic and lithological traps, and that these rocks should be the targets of future exploration. Yao et al. (2013) studied the sedimentary characteristics of the Longwangmiao Formation, identifying four types of dolostone (dolarenite, oolitic dolomite, crystalline dolostone and porphyritic dolomite), and three sedimentary facies (shoal, shoal wing and shoal flat), in which the shoal facies dolomite was shown to be the most effective oil–gas reservoir. Further studies by Li et al. (2014b) characterized the Longwangmiao reservoir and showed that this is predominantly a pore-type reservoir in the shoal facies, with areas of pore-type reservoir developed by karstification in the Caledonian. Studies of the composition, light hydrocarbon characteristics and carbon isotopes of the gas indicate that the formation of natural gas resulted from oil cracking, which was likely derived from the underlying Lower Cambrian Qiongzhusi Formation (Wei et al., 2014; Zheng et al., 2014; Zou et al., 2014a). Xu et al. (2014) proposed that multiple source rocks, reservoirs, and traps occur in the Leshan–Longnvsi paleo-uplift, which together form a Cambrian–Neoproterozoic petroleum system.

The hydrocarbon source(s) and accumulation process of the Longwangmiao reservoir is the key to understanding this gas system and shaping gas exploration strategies. In previous studies, the Lower Cambrian Qiongzhusi shales were believed to be the only source for the Longwangmiao reservoir, because they underly the Longwangmiao reservoir closely (Fig. 3), and both the Longwangmiao and underlying Dengying gases are oil-cracking in origin (Wei et al., 2014; Zheng et al., 2014; Zou et al., 2014a). However, in light of recent exploration and research findings, these understandings were challenged: (1) First, the highest temperature that the Dengying and Longwangmiao reservoirs have been subjected to are different, i.e., over 200 °C and around 170 °C, respectively. As a consequence, oil cracking may only take place in the Dengying reservoir, but not in the Longwangmiao reservoir; (2) furthermore, based on the geological setting, the high-quality source rock unit of the Lower Silurian Longmaxi Formation shale (Liu et al., 2012; Tenger et al., 2014) can act as another candidate of hydrocarbon source for the Longwangmiao gas in addition to the commonly acknowledged Qiongzhusi shale (Fig. 3). The older Longwangmiao reservoir is in uplift areas and contact with the younger Longmaxi source rocks in sag areas extends directly in a lateral direction (Xu et al., 2014; Fig. 3). Thus, it is possible for the Longmaxi-generating petroleum to migrate into the Longwangmiao reservoir, forming a somewhat non-traditional combination of an older reservoir and younger source rocks (Fig. 3). This pattern is different from that of the underlying Dengying gas reservoir; (3) furthermore, the geochemical characteristics of the gas and bitumen in the Longwangmiao and Dengying reservoirs are different (Dai et al., 2000; Dai, 2003; Zhu et al., 2006, 2007; Sun et al., 2010). Gases of the Longwangmiao and the Dengying reservoirs in the Gaoshiti–Moxi area show separated and different characteristics, such as $\delta^{13}C_2$ values ranging from −35.3‰ to −32.3‰ and −29.5‰ to −26.8‰, respectively (Wei et al., 2014, 2015; Zou et al., 2014b). The bulk $\delta^{13}C$ values of extracted bitumen from the two reservoirs is also different (Longwangmiao = −28.4‰ to −25.6‰; Dengying = −28.8‰ to −28.0‰; this study). This implies different source rocks and/or hydrocarbon accumulation processes of these gases/bitumens. Such differences will require different hydrocarbon accumulation models and exploration programs.

To substantiate this hypothesis, this study presents new organic petrological and geochemical results on recovered bitumens. We chose bitumen as the object of study because it occurs widely in the Longwangmiao reservoir and has important implications for understanding the hydrocarbon accumulation processes of this gas reservoir. Previous research has suggested that the Longwangmiao bitumen is also of oil-cracking origin like the underlying Dengying bitumen and thus few studies have been conducted on the bitumen. However, as outlined above, the Longwangmiao and Dengying bitumens may have different origins. This needs to be clarified. Overall, the key aim of this study is to decide whether or not the Longwangmiao and Dengying gas reservoirs, which are separated by the Qiongzhusi shales, do in fact share the same bitumen/gas origin and hydrocarbon accumulation process (Fig. 3).

2. Geological setting

2.1. Structural evolution of the study area

The Longwangmiao gas field is located in the Gaoshiti–Moxi area in the central part of the Sichuan Basin, which is also termed the Chuanzhong area in Chinese (Fig. 1a). The Sichuan Basin is located in southwestern China, and is a superimposed petroliferous basin developed on the Precambrian Yangtze Craton basement (Wang, 1995; Guo et al., 1996; Li et al., 1997; Hou et al., 1999; Xu et al., 2012; Wang et al., 2014; Li et al., 2014a). The basin can be divided into six structural units, which are the Western Sichuan Depression (I), and the Northern Sichuan Low-lying and Flat (II), Central Sichuan Flat (III), Southwestern Sichuan Low-lying and Sharp (IV), Southeastern Sichuan High and Sharp (V), and Southern Sichuan Low-lying and Sharp fold belts (VI) (Yang et al., 2002; Wei et al., 2005; Xu et al., 2006; Shen et al., 2007; Fig. 1a).

The Longwangmiao gas field in the Gaoshiti–Moxi area (part of the Chuanzhong area) is located in the Leshan–Longnvsi paleo-uplift (Fig. 1a), which is a large skirt-shaped structure that formed early as a result of the Tongwan movement during the Caledonian Orogeny (Huang, 2009). Following the end of the Caledonian Orogeny, the structure was not affected by severe tectonic movements whereas it was slightly affected by syn-sedimentary uplift and erosion (Guo et al., 1996; Xu and Xiong, 1999; Li et al., 2001).

During the Devonian–Permian Hercynian Orogeny, basin uplift caused erosion of Cambrian–Silurian strata and the formation of karst reservoirs in Cambrian and Ordovician carbonate rocks (Bureau of Geology and Mineral Resources of Sichuan Province, 1991; Liu and Xu, 1994; Li et al., 2011). Regional sedimentation followed, resulting in deposition of Early Permian carbonates overlying the Lower Paleozoic weathered surface from the Caledonian paleo-uplift. These regional sediments, including Late Permian coal shales, formed regional seals above the unconformity produced by the paleo-uplift (Feng, 1991; He et al., 2005).

The western part of the paleo-uplifted area remained relatively stable during the Triassic–Jurassic (Indosinian and Early–Middle Yanshanian orogenies), whereas the eastern part moved southward as a result of the Luzhou paleo-uplift (Deng, 1992). Since the Cretaceous (Late Yanshanian and Himalaya orogenies), the eastern part of the paleo-uplift has remained relatively stable with some uplift during the Himalaya Orogeny, whereas regional folding has caused the southward movement of the western part with strong folding and uplift during the Himalaya Orogeny (Tong, 2000; Li et al., 2014a).

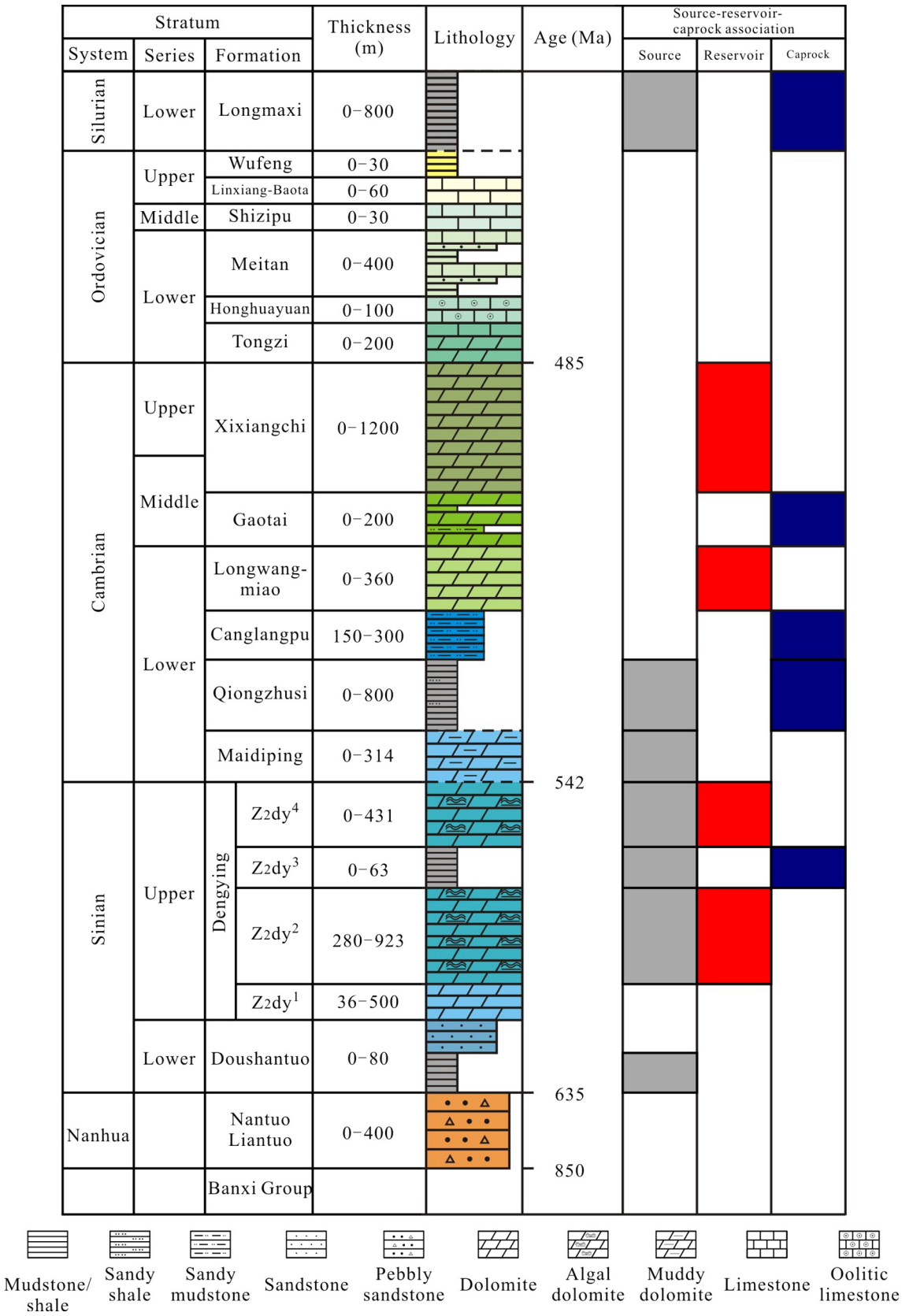

Fig. 2. Stratigraphy and source–reservoir–caprock relationships of the Sinian Dengying and Lower Cambrian Longwangmiao natural gas systems in the Sichuan Basin.

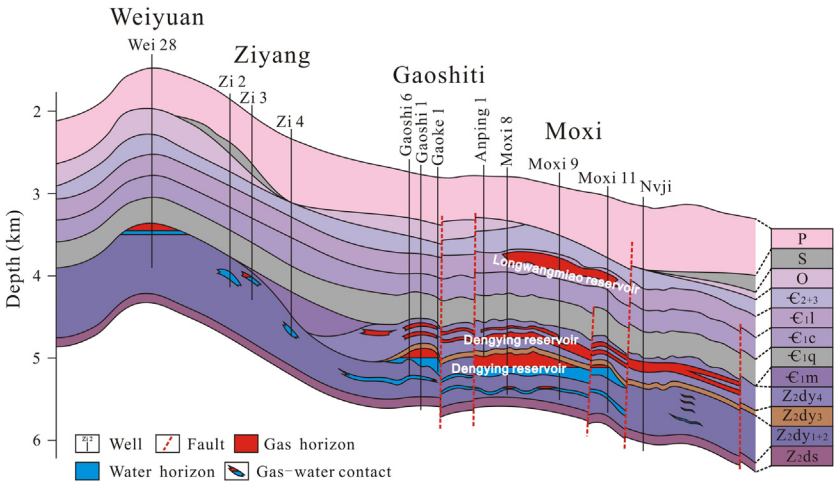

Fig. 3. Well cross-section through the Dengying and Longwangmiao gas accumulations in the Leshan–Longnvsi paleo-uplift. See Fig. 1a for the location of the cross-section. Z_2ds: the Sinan Doushantuo Formation; Z_2dy_{1+2}: the first and second members of the Sinian Dengying Formation; Z_2dy_3: the third member of the Sinian Dengying Formation; Z_2dy_4: the fourth member of the Sinian Dengying Formation; ϵ_1m: the Lower Cambrian Maidiping Formation; ϵ_1q: the Lower Cambrian Qiongzhusi Formation; ϵ_1c: the Lower Cambrian Canglangpu Formation; ϵ_1l: the Lower Cambrian Longwangmiao Formation; ϵ_{2+3}: the Middle and Upper Cambrian; O: Ordovician; S: Silurian; P: Permian.

2.2. Overview of petroleum exploration and possible source rocks

Most of the Longwangmiao reservoirs are found in dolostones of the Moxi area (Figs. 1 and 2). Well Moxi 8 generates natural gas at approximately 2×10^6 m^3/day, and contains approximately 440×10^9 m^3 of explored gas reserves (Zou et al., 2014a). Based on the geological setting, the Longwangmiao gas may have been sourced from multiple sources as outlined above, mainly including the Lower Cambrian Qiongzhusi and Lower Silurian Longmaxi formations. This differs from gas accumulations in the Dengying reservoir, where only the Qiongzhusi Formation acted as the dominant source (Fig. 3).

Fig. 4a shows the regional distribution of the Lower Cambrian Qiongzhusi Formation, which consists of black–gray mudstone or shale deposited in a gulf. The mudstone/shale ranges from 0 to 160 m in thickness, and is thickest in the southern and northwestern basin and relatively thin (20–80 m) in the central part of the Sichuan Basin (Xu et al., 2000; Cheng et al., 2009; Li et al., 2009; Wang et al., 2009; Zou et al., 2015). The abundance of organic matter in the shales is regionally variable, with the highest total organic carbon (TOC) contents occurring in the Central basin and Weiyuan–Ziyang areas (TOC > 2.0%), and the lowest TOC found in the southwestern parts of the Sichuan Basin (TOC < 1.0%). Thus, there may have been two separate hydrocarbon-generating centers for the Central Basin and the Weiyuan–Ziyang region, respectively (Zou et al., 2015).

The Lower Silurian Longmaxi Formation also consists of black–gray shale deposited in a gulf (Fig. 4b). This shale ranges in thickness from 0 to 120 m, and contains two hydrocarbon-generating centers, one in the Luzhou–Zigong–Yibin–Chongqing belt in southern Sichuan Basin (TOC ~ 1.0%), and the second in the Shizhu–Wanzhou area in the eastern part of the basin (TOC > 2.0%; Zou et al., 2015).

These source rocks have complex burial and thermal evolution histories, which would result in complex hydrocarbon generating processes. The evolution of the Qiongzhusi Formation can be divided into four stages in general (Fig. 5). Stage I (Ordovician–Silurian) represents the initial hydrocarbon generation stage, with organic matter of low maturity (%Ro = 0.5–0.7). Stage II (Silurian to pre-Permian) was marked by a cessation in hydrocarbon generation, and the erosion of Ordovician–Silurian supra-crustal rocks caused by uplift during the Caledonian Orogeny. Stage III (Triassic to Middle Jurassic) represents the second stage of hydrocarbon generation when supra-crustal successions were reburied, and peak hydrocarbon generating conditions were reached late in the Triassic (%Ro = 0.7–1.3). Stage IV began in the Middle Jurassic and

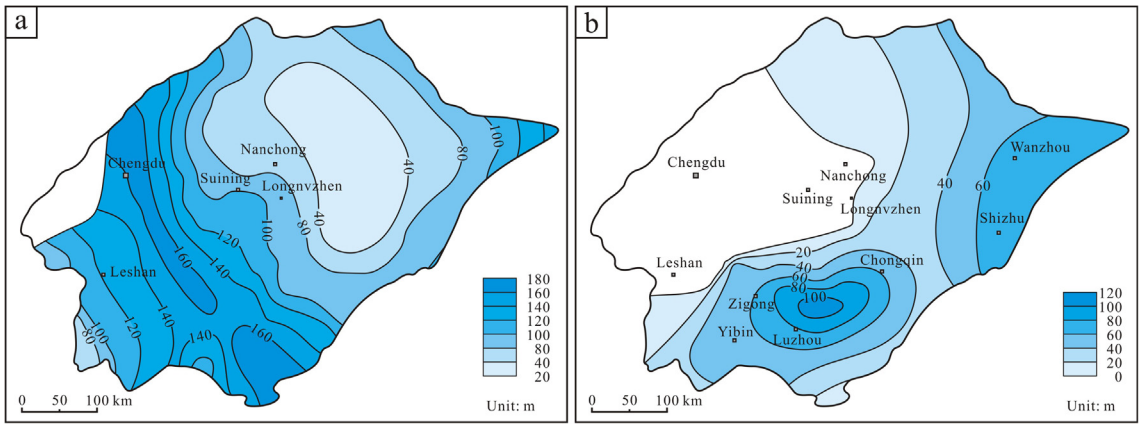

Fig. 4. Distribution of possible source rocks of the: (a) Qiongzhusi shale, and (b) Longmaxi shale (modified after Zou et al., 2015).

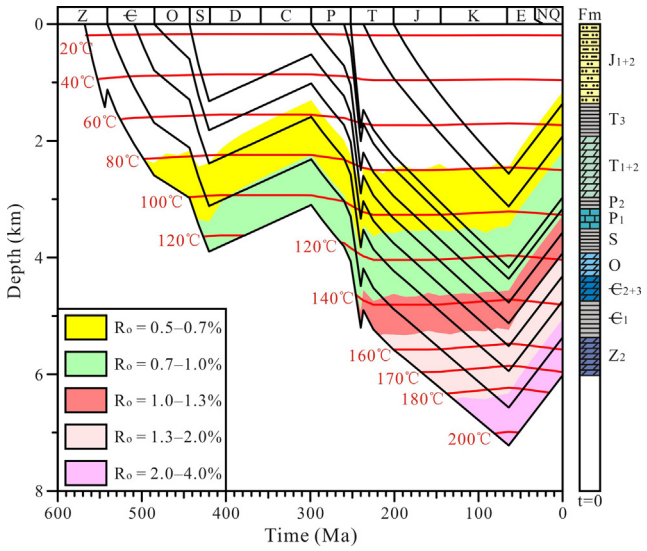

Fig. 5. Stratigraphic burial and organic matter thermal evolution in the Gaoshiti–Moxi area of the Sichuan Basin.

was a gas generation stage, which can be divided into wet (Jurassic–Late Cretaceous; %Ro = 1.3–2.0) and dry (Cretaceous–present; %Ro = 2.0–4.0) gas stages based on the maturity of organic matter. In contrast, for the Lower Silurian Longmaxi source rocks, the Caledonian Orogeny caused the shallow burial of the rocks prior to the Triassic, resulting in a low level of thermal evolution and low maturity of organic matter. The Longmaxi Formation experienced two tectonic stages (Fig. 5). The first was during the early Triassic to early Jurassic (Stage I), producing petroleum of low maturity (% Ro = 0.5–0.7). The second was after the Middle Jurassic to the present, resulting in organic matter reaching the oil generating stage (Stage II; %Ro = 0.7–1.3), with peak conditions being reached in the Middle Cretaceous.

3. Samples and methods

3.1. Samples

Twelve bituminous reservoir dolomite samples and one bitumen sample from the Longwangmiao reservoir were collected from six wells in the Moxi area (Moxi 7, 11, 12, 13, 17, and 19), and two wells in the Gaoshiti area (Gaoshi 6 and 10) adjacent to the Moxi area (Fig. 1; Table 1). For comparison with the Dengying reservoir, three bituminous reservoir dolomites and two bitumen samples were collected from three wells in the Gaoshiti–Moxi area (Gaoshi 1, Gaoke 1 and Anping 1; Fig. 1; Table 1).

Note that the sample set should be as large as possible to justify a total oil-source correlation in theory. However, this cannot be satisfied in many circumstances like in this study because drill coring is commonly selective and samples are valuable for research. To compensate, the data of source rocks in this study are all from the depositional center.

The Longwangmiao reservoir produces only gas with no crude oils, and thus we can only use reservoir bitumen samples for correlation. Results show that few in situ compounds were present because the results are consistent with the geology, or there should be inconsistencies (see Results and Discussion sections).

3.2. Methods

3.2.1. Petrology

Samples were examined under transmitted, reflected and fluorescent light using a Nikon ECLIPSE LV100NPOL microscope for organic petrology analysis. The light sources of the transmitted and reflected lights were a 100 W halogen lamp, while the source of the fluorescence light was a 100 W mercury lamp, and photomicrographs were obtained by a Nikon DS-Ri1 digital micrography and imaging system. Organic petrology was conducted in order to identify bitumen and oil–gas charging in the samples.

Reflectance of bitumen (R_b) was determined using a Zeiss Axioskop 40Pol microscope equipped with MSP210 spectrophotometer. R_b values were analyzed to determine the maturity of bitumen.

3.2.2. Organic geochemistry

Organic geochemical analysis was conducted on chloroform extracts from the reservoir bitumen. The pretreatment methods refer to China National Oil and Gas Standard SY/T 5118-2008 and SY/T 5238-2008. Briefly, samples were first cleaned with distilled water to remove any weathering products. They were then crushed to 80 mesh and ca. 50 g was Soxhlet extracted with chloroform for 72 h.

Carbon isotope ($\delta^{13}C$) compositions were determined using a MAT 253 instrument under the following conditions: energy = 68 eV, mass resolution = 200, vacuum < 2×10^{-6} Pa, and emission current = 0.8 mA. Vienna Pee Dee Belemnite (VPDB) was used

Table 1
Sample information, reflectance of bitumen (R_b), and carbon isotope data for samples from the Longwangmiao and Dengying reservoirs.

No.	Sample	Well	Depth (m)	Formation	Type	R_b (%)	Carbon isotope ($\delta^{13}C$, VPDB, ‰)
1	GS6-2	Gaoshi 6	4548.3	Longwangmiao	Reservoir extracted bitumen	2.42	−25.7
2	GS10-215	Gaoshi 10	4627.9			2.48	−26.8
3	MX7-143	Moxi 7	4638.1			2.57	−27.2
4	MX11-2	Moxi 11	4877.0			2.95	−25.6
5	MX12-2	Moxi 12	4621.8			3.67	−27.7
6	MX12-98	Moxi 12	4632.6			3.33	−25.7
7	MX12-103	Moxi 12	4655.2			2.39	−26.2
8	MX13-57	Moxi 13	4579.7			2.60	−26.0
9	MX13-73	Moxi 13	4615.8			3.39	−26.8
10	MX17-134	Moxi 17	4623.3			3.23	−28.0
11	MX17-148	Moxi 17	4649.5			2.28	−26.5
12	MX19-195	Moxi 19	4658.1			2.19	−28.4
13	MX12B-1	Moxi 12	4625.0		Pure bitumen	3.42	−26.7
14	GSB-1	Gaoshi 1	4960.3	Dengying	Reservoir extracted bitumen	4.20	−28.6
15	GKB-1	Gaoke 1	5031.5			3.49	−28.8
16	APB-1	Anping 1	5053.3			3.90	−28.0
17	GKB-2	Gaoke 1	5178.3		Pure bitumen	3.71	−28.7
18	APB-3	Anping 1	5040.8			4.02	−28.3

as the analytical standard, and all data have a precision better than ± 0.1‰.

Alkane and biomarker analyses include gas chromatography (GC) and gas chromatography–mass spectrometry (GC–MS) analyses of the saturated fraction of the chloroform extract. Analysis of aromatic hydrocarbons was not conducted due to their extremely low abundance. These analyses of saturated hydrocarbons were conducted with an HP 6890 chromatograph fitted with a DB-5 capillary column (25 m × 0.20 mm × 0.33 μm). The GC oven temperature was initially at 60 °C and then increased to 310 °C at 7 °C/min, where it was held for 20 min. Helium was used as a carrier gas, with a flow rate of 1 mL/min. An Agilent 5973 interfaced with an HP 6890 chromatograph fitted with a DB-5MS capillary column (30 m × 0.25 mm × 0.25 μm) was used for GC–MS analysis. The GC oven temperature was initially held at 80 °C for 3 min before being increased to 230 °C at 3 °C/min, and then to 310 °C at 2 °C/min, where it was held for 15 min. Helium was used as a carrier gas, with a flow rate of 1 mL/min. The mass spectrometer was operated at 70 eV, with an ion source temperature of 230 °C. The temperature of the transmission line was 300 °C. The effluent of the column was monitored in multiple ion detection (MID) mode.

In addition, as outlined above, one of the critical issues for clarifying the origin of the Longwangmiao gas/bitumen is if the gas is oil-cracking and the bitumen is consequently pyrobitumen. To ascertain this, the solubility of the samples in CS_2 solvents should be tested. However, such an experiment could not be conducted in this study because there is a mix of relatively mature oil bitumen

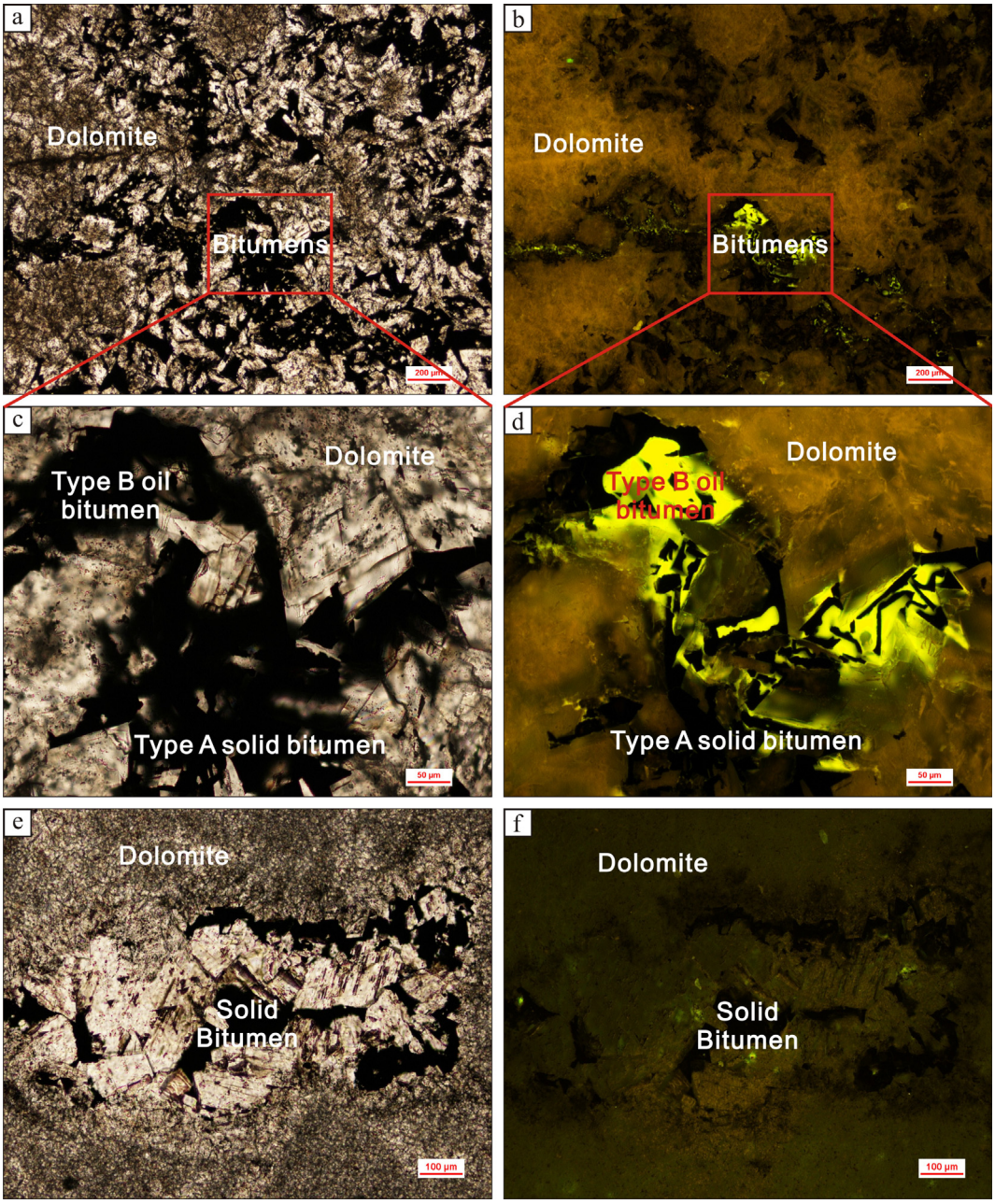

Fig. 6. Photomicrographs showing the organic petrological characteristics of: (a and b) solid bitumen and oil bitumen in the Longwangmiao reservoir under plane polarized and fluorescence lights, respectively (sample MX12-2); (c and d) oil bitumen in the Longwangmiao reservoir under plane polarized and fluorescence lights, respectively (red frame in Fig. 1a and b); (e and f) solid bitumen in the Dengying reservoir under plane polarized and fluorescence lights, respectively (sample GKB-1). See Fig. 1 and Table 1 for the location and basic information of the samples, respectively.

with relatively highly mature bitumen in the reservoir based on petrological results (Section 4.1). Thus, the results of the CS_2 experiment, if conducted, would be a mix of different end-member bitumens and cannot reflect the original characteristics of the end-member bitumens. Considering this, we did not run the experiment.

3.2.3. Inorganic (element) geochemistry

The trace elements of the pure reservoir bitumen were analyzed using the methods of Akinlua et al. (2008, 2015), with the aim of hydrocarbon–source correlation. The pure bitumen samples were prepared as follows: After we obtained the bitumen from the reservoir rocks, we checked it carefully under the microscope and made sure that there were no mineral grains present. Then, we washed them with Milli-Q water at least three times. Last, we put them in oven for 4 h under 50 °C to remove water (e.g., Olsen et al., 1995). Then, approximately 0.03 g of bitumen from each sample was transferred into sealable 10 mL Teflon cups, treated with 0.2 mL of distilled HF and 3 mL of distilled HNO_3, and digested at 185 °C for 12 h in a drying oven. Each cup was cooled to room temperature, opened and then dried on a hot plate at 160 °C. The residue was dissolved in a mixture of 2 mL of HNO_3 and 4 mL of distilled water, and 100 ng of Rh (in-house standard) was added. The cups were then heated on a hot plate to accelerate dissolution. The solution containing each sample was then transferred into 15 mL centrifuge tubes, and filled to 10 mL with distilled water for the measurement of trace elements by ICP–MS.

4. Results

4.1. Organic petrology

Petrological observations show that the Longwangmiao Formation is composed predominantly of dolomite, although dolomite grains have been recrystallized to varying degrees during long diagenesis. The dolomite is characterized by intergranular dissolution pores, with diameters from several tens to hundreds of microns. The pore spaces are filled by bitumens, including high maturity bitumen (termed Type A solid bitumen in this study) and low maturity bitumen (termed Type B oil bitumen in this study), which can be differentiated by fluorescence and reflectance (Fig. 6a–d; see discussion in Section 5.1 for details).

The Type A solid bitumen transmits little light and is not highly fluorescent. This implies that it is relatively highly to over-mature. It occurs predominantly in dissolution pores and constitutes ~ 90% of all bitumen in the field of view (Fig. 6a and b). In contrast, the Type B oil bitumen is brown–black in color in plane-polarized light, and fluoresces yellow–green. This implies that it is relatively mature. It occurs within residual spaces in the Type A bitumen, and constitutes ~ 10% of the total bitumen in the field of view (Fig. 6a and b). Therefore, it can be deduced that the Type A solid bitumen was charged earlier than the Type B oil bitumen and is the dominant type. The bitumen reflectance (R_b) of the Type A solid bitumen ranges from 2.19% to 3.67% (mean = 2.79%; Table 1), further supporting the high maturity of this bitumen. It can be classified as solid bitumen according to Tissot and Welte (1984). The R_b of later-charged Type B oil bitumen could not be determined, indicating that it is of low maturity. Thus, it is oil bitumen (Tissot and Welte, 1984).

In contrast to the Longwangmiao bitumen, that of the Dengying reservoir is highly to over-mature bitumen (Fig. 6e and f), which shares similar characteristics with the Type A solid bitumen in the Longwangmiao reservoir, including dark to black color in transmitted and fluorescent lights, R_b values (R_b = 3.49–4.20%, mean = 3.86%; Table 1), and occurrence mainly in dissolution pores of the dolomite (Fig. 6e and f). Such bitumens are solid bitumen to pyrobitumen (Huang and Ran, 1989; Huang and Chen, 1993; Hu et al., 2007).

4.2. Organic geochemistry

4.2.1. Carbon isotopes

Table 1 lists the carbon isotope ($\delta^{13}C$) values of extracted bitumen from the Longwangmiao and Dengying reservoir samples. The Longwangmiao $\delta^{13}C$ values range from −28.4‰ to −25.6‰ (mean $\delta^{13}C$ = −26.7‰), whereas values from Dengying are slightly depleted, ranging from −28.8‰ to −28.0‰ (mean $\delta^{13}C$ = −28.5‰).

4.2.2. Alkanes, isoprenoids and biomarkers

A variety of *n*-alkanes, isoprenoids and biomarkers (terpanes and steranes) were detected in the reservoir samples of this study. We calculated ratios of these alkanes, isoprenoids and biomarkers based on relative abundance, which can reflect the source, depositional environment and maturity of organic matter (Peters et al., 2005), with the aim to identifying any differences in the bitumens in the Longwangmiao and Dengying reservoirs and whether they are sourced from same source rock units.

4.2.2.1. Alkanes and isoprenoids. The *n*-alkanes detected in the Longwangmiao samples are predominantly in the range n-C_{14}–n-C_{38}, although small amounts of n-C_{13}, n-C_{39}, and n-C_{40} alkanes were identified. Light-end *n*-alkanes have a relatively low abundance.

Table 2
Geochemical characteristics of alkanes and isoprenoids in the reservoir extracted bitumen.

No.	Sample	Peak Position 1	Peak Position 2	n-C_{21}^{-}/n-C_{22}^{+}	OEP	Pr/Ph	Pr/n-C_{17}	Ph/n-C_{18}
1	GS6-2	C_{23}	C_{29}	0.30	1.08	0.44	1.23	1.64
2	GS10-215	C_{21}	C_{27}	0.82	1.03	0.79	0.44	0.29
3	MX7-143	C_{19}	C_{27}	0.90	1.05	0.84	0.40	0.29
4	MX11-2	C_{19}	C_{27}	0.94	1.01	0.98	0.85	0.72
5	MX12-2	C_{20}	C_{27}	0.85	1.02	0.76	0.44	0.36
6	MX12-98	C_{20}	C_{27}	0.60	1.02	0.54	0.36	0.29
7	MX12-103	C_{19}	C_{27}	1.02	1.10	0.46	0.51	0.34
8	MX13-57	C_{21}	C_{27}	0.55	1.01	0.59	0.64	0.60
9	MX13-73	C_{21}	C_{27}	0.65	1.04	0.57	0.52	0.35
10	MX17-134	C_{20}	C_{27}	1.17	1.04	0.47	0.46	0.50
11	MX17-148	C_{22}	C_{27}	0.41	1.02	0.32	0.86	0.89
12	MX19-195	C_{19}	C_{27}	0.97	1.02	0.73	0.60	0.58
13	GSB-1	C_{19}	/	2.70	1.00	0.96	0.71	0.66
14	GKB-1	C_{18}	/	2.78	1.00	0.73	0.57	0.61
15	APB-1	C_{19}	/	1.54	0.97	0.42	1.12	1.36

Note: n-C_{21}^{-}/n-C_{22}^{+} = (n-C_{21} + n-C_{20} + n-C_{19} + ...)/(n-C_{22} + n-C_{23} + n-C_{24} + ...); OEP (odd over even carbon preference) = (n-C_{21} + 6 × n-C_{23} + n-C_{25})/(4 × n-C_{22} + 4 × n-C_{24}); "/" denotes not applicable.

The majority of the samples show two peaks of *n*-alkanes at *n*-C_{19}–*n*-C_{22}, and *n*-C_{27} and *n*-C_{29} (Table 2; Fig. 7a). The *n*-C_{21}^{-}/*n*-C_{22}^{+} values range from 0.30 to 1.17 (mean *n*-C_{21}^{-}/*n*-C_{22}^{+} = 0.77; Table 2), and the OEP values range from 1.01 to 1.10 (mean OEP = 1.04; Table 2). Isoprenoids including pristane and phytane were detected in all samples: pristane/phytane (Pr/Ph) = 0.32–0.98 (mean Pr/Ph = 0.62), Pr/*n*-C_{17} = 0.36–1.23 (mean Pr/*n*-C_{17} = 0.61), and Ph/*n*-C_{18} = 0.29–1.64 (mean Ph/*n*-C_{18} = 0.57; Table 2). Note that the Pr/Ph ratio might be somewhat lower than the original value due to the evaporative loss of light-end *n*-alkanes and thus has not been used for addressing geological and geochemical implications.

Alkanes and isoprenoids in the Dengying samples show different characteristics to the Longwangmiao samples. *n*-Alkanes consist of *n*-C_{16}–*n*-C_{32} homologs showing one peak around *n*-C_{18} and *n*-C_{19} (Fig. 7e). Their *n*-C_{21}^{-}/*n*-C_{22}^{+} values range from 1.54 to 2.78,

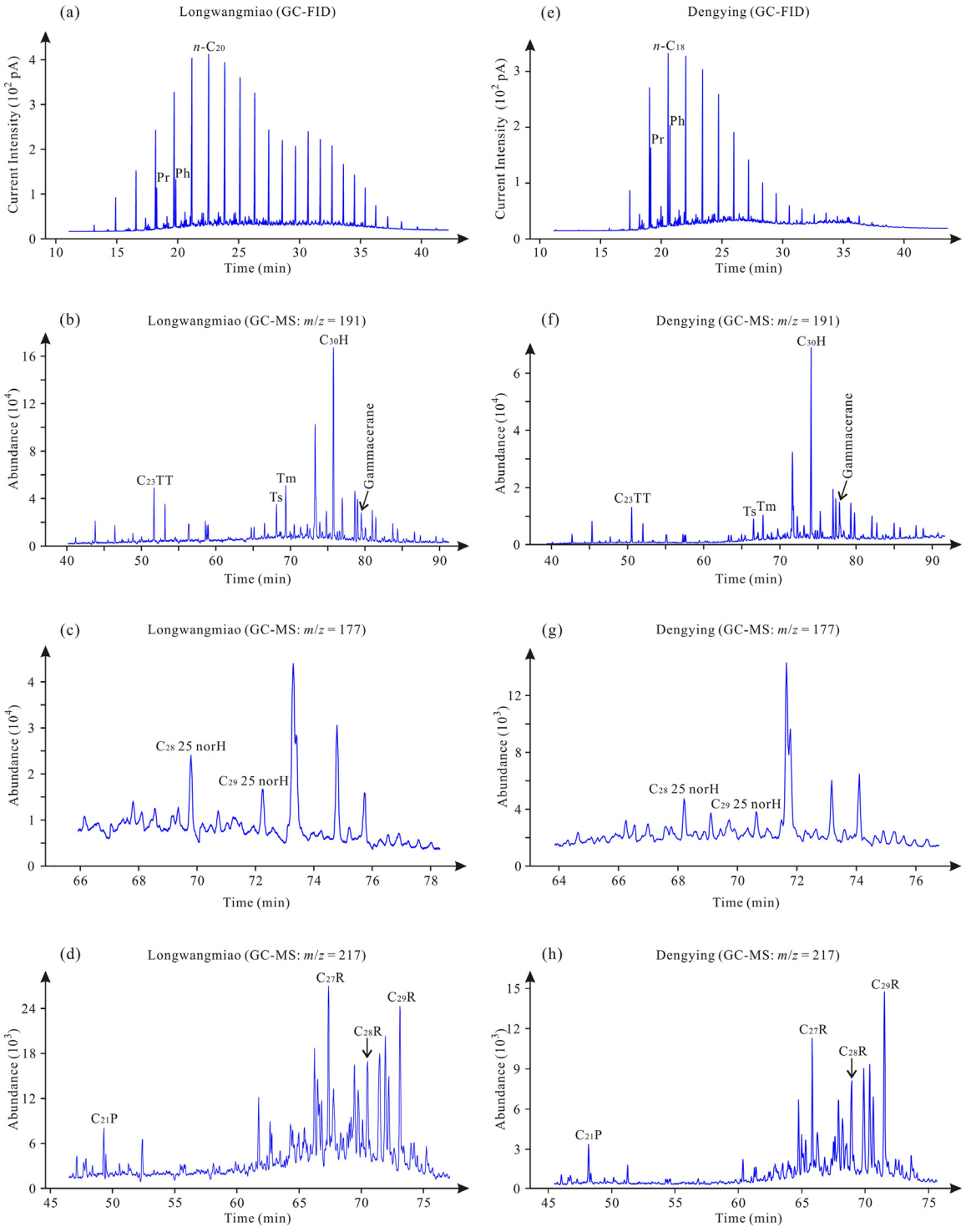

Fig. 7. GC-FID and GC–MS spectra of reservoir bitumen showing compositions of: (a–d) sample MX12-2 and (e–h) sample GKB-1. TT: tricyclic terpane; H: pentacyclic triterpane (hopane); Ts: 18α(H)-22,29,30-trinorhopane; Tm: 17α(H)-22,29,30-trinorhopane; norH: norhopane; P: C_{21} sterane; in (d) and (h) the 20R α,α,α-steranes isomers are labeled.

Table 3
Geochemical characteristics of terpanes in the reservoir extracted bitumen.

Sample	TT 22/21	TT 24/23	TT 26/25	TeTT	TT_{23}/H_{30}	$H_{31}R/H_{30}$	Nor H_{29}/H_{30}	Ts/Tm	G/H_{30}	Dia H_{30}/H_{30}	$H_{31}SR$
GS6-2	0.31	0.77	0.80	0.20	0.35	0.37	/	1.00	0.37	0.14	0.44
GS10-215	0.31	0.68	1.20	0.41	0.12	0.21	0.06	0.65	0.16	0.08	0.53
MX7-143	0.34	0.65	1.23	0.38	0.08	0.21	0.06	0.73	0.17	0.08	0.55
MX11-2	0.25	0.52	0.72	0.52	0.36	0.33	/	0.15	0.15	0.04	0.45
MX12-2	0.48	0.61	1.05	0.40	0.21	0.22	0.07	0.65	0.16	0.10	0.54
MX12-98	0.32	0.62	0.88	0.40	0.32	0.24	0.07	0.34	0.14	0.07	0.53
MX12-103	0.32	0.63	1.04	0.37	0.23	0.22	0.07	0.56	0.17	0.08	0.54
MX13-57	0.29	0.61	0.94	0.49	0.21	0.28	0.05	0.25	0.13	0.05	0.48
MX13-73	0.28	0.64	1.17	0.48	0.10	0.22	0.04	0.37	0.24	0.05	0.49
MX17-134	0.34	0.64	1.17	0.37	0.12	0.21	0.06	0.83	0.16	0.07	0.54
MX17-148	0.23	0.62	1.04	0.42	0.14	0.23	0.06	0.54	0.15	0.07	0.53
MX19-195	0.30	0.62	1.07	0.39	0.13	0.20	0.07	0.65	0.13	0.07	0.53
GSB-1	0.26	0.67	1.25	0.43	0.10	0.17	0.06	1.01	0.09	0.09	0.55
GKB-1	0.28	0.56	1.11	0.37	0.13	0.23	0.03	0.83	0.21	0.13	0.54
APB-1	0.32	0.62	1.12	0.33	0.15	0.20	0.04	0.70	0.29	0.07	0.55

Note: "/" denotes value below detection limits.
TT 22/21: C_{22} tricyclic terpane/C_{21} tricyclic terpane; TT 24/23: C_{24} tricyclic terpane/C_{23} tricyclic terpane; TT 26/25: C_{26} tricyclic terpane/C_{25} tricyclic terpane; $H_{31}R/H_{30}$: $C_{31}R$ hopane/C_{30} hopane; TeTT: C_{24} tetracyclic terpane/(C_{24} tetracyclic terpane + C_{26} tricyclic terpane); TT_{23}/H_{30}: C_{23} tricyclic terpane/C_{30} hopane; Nor H_{29}/H_{30}: C_{29} 25-norhopane/C_{30} hopane; G/H_{30}: gammacerane/C_{30} hopane; Dia H_{30}/H_{30}: C_{30} diahopane/C_{30} hopane; $H_{31}SR$: hopane C_{31} 22S/(22S + 22R).

Table 4
Geochemical characteristics of steranes in the reservoir extracted bitumen.

Sample	TriαS 27R %	TriαS 28R %	TriαS 29R %	TriαS 27/29R	TriαS 29SR	S29αβ	RS/H	DiaS/RS
GS6-2	31%	27%	42%	0.72	0.48	0.45	0.73	0.43
GS10-215	34%	27%	39%	0.87	0.46	0.40	0.37	0.29
MX7-143	33%	27%	40%	0.83	0.49	0.41	0.34	0.26
MX11-2	33%	29%	38%	0.86	0.36	0.34	0.29	0.26
MX12-2	37%	27%	36%	1.01	0.50	0.43	0.36	0.33
MX12-98	34%	27%	39%	0.89	0.47	0.41	0.30	0.34
MX12-103	33%	29%	38%	0.87	0.45	0.37	0.36	0.29
MX13-57	34%	27%	39%	0.87	0.45	0.39	0.23	0.31
MX13-73	26%	29%	45%	0.58	0.39	0.34	0.28	0.23
MX17-134	35%	27%	38%	0.90	0.48	0.41	0.35	0.27
MX17-148	34%	27%	39%	0.87	0.47	0.40	0.33	0.29
MX19-195	33%	29%	38%	0.86	0.47	0.37	0.33	0.26
GSB-1	32%	28%	40%	0.80	0.53	0.43	0.29	0.35
GKB-1	27%	26%	47%	0.58	0.42	0.36	0.41	0.19
APB-1	27%	27%	46%	0.58	0.45	0.37	0.41	0.18

Note: TriαS27R %: sterane C_{27} ααα20R/(sterane C_{27} ααα20R + sterane C_{28} ααα20R + sterane C_{29} ααα20R) × 100%; TriαS28R %: sterane C_{28} ααα20R/(sterane C_{27} ααα20R + sterane C_{28} ααα20R + sterane C_{29} ααα20R) × 100%; TriαS29R %: sterane C_{29} ααα20R/(sterane C_{27} ααα20R + sterane C_{28} ααα20R + sterane C_{29} ααα20R) × 100%; TriαS27/29R: steranes C_{27} ααα20R/C_{29} ααα20R; TriαS29SR: sterane C_{29} ααα20S/(20S + 20R); S29αβ: sterane C_{29} ββ/(ββ + αα); RS/H: regular steranes/hopanes; DiaS/RS: diasteranes/regular steranes.

Table 5
Trace element compositions of the reservoir pure bitumen and PAAS.

Elements	Samples			
	PAAS	MA12B-1	GKB-2	APB-3
Sc (ppm)	16.0	4.4	0.42	0.31
Rb (ppm)	160	17.1	4.0	2.65
Zr (ppm)	210	58	2.06	0.40
Nb (ppm)	19.0	4.0	0.24	0.02
Cs (ppm)	5.00	0.33	0.05	0.02
Hf (ppm)	5.00	1.42	0.03	0.01
Th (ppm)	14.6	3.8	0.16	0.02
Ga (ppm)	20.0	3.9	0.65	0.24
V (ppm)	150	222	173	335
Ni (ppm)	55.0	77	104	197
U (ppm)	3.10	5.2	0.87	0.08
Cr (ppm)	110	40	13.2	6.6
Co (ppm)	23.0	4.7	0.55	0.30
Pb (ppm)	20.0	113	38	19.6
Sr (ppm)	200	122	20.1	25.0
Ba (ppm)	650	989	1290	18.8
Total (ppm)	1661	1666	1647	606
V/(V + Ni)	0.73	0.74	0.62	0.63
Ni/Co	2.4	16.4	189	657
V/Cr	1.4	5.6	13.1	50.8
U/Th	0.2	1.4	5.4	4.0

averaging 2.34, and the OEP values are 0.97–1.00 (mean OEP = 0.99). Pristane and phytane were detected in all samples: Pr/Ph = 0.42–0.96 (mean Pr/Ph = 0.70), Pr/*n*-C_{17} = 0.57–1.12 (mean Pr/*n*-C_{17} = 0.80), and Ph/*n*-C_{18} = 0.61–1.36 (mean Ph/*n*-C_{18} = 0.88).

4.2.2.2. Terpanes. Terpanes, including tricyclic and tetracyclic terpanes and pentacyclic triterpanes (hopanes), were identified in the Longwangmiao samples (Table 3; Fig. 7b and c). Tricyclic terpanes include C_{19}–C_{30} terpanes, and typically $C_{20} < C_{21} < C_{23}$ in all samples, with the exception of sample MX12-2. The chromatograms show peaks at C_{23}, with C_{23} tricyclic terpane/C_{30} hopane = 0.08–0.36 (mean = 0.20; Table 3). C_{24} tetracyclic terpanes are present in all of the Longwangmiao samples, with C_{24} tetracyclic terpane/(C_{24} tetracyclic terpane + C_{26} tricyclic terpane) = 0.20–0.52 (mean = 0.40; Table 3). The C_{27}–C_{35} hopanes within the Longwangmiao samples show a peak abundance at C_{30}. All C_{31}–C_{35} hopanes have expected isomers, and relative concentrations decrease gradually from C_{31} to C_{35}. Other common compounds include C_{30} diahopane, Ts (18α(H)-22,29,30-trinorhopane), Tm (17α(H)-22,29,30-trinorhopane), and gammacerane. In addition, C_{29} 25-norhopanes were identified in the *m*/*z* = 177 mass chromatograms (Fig. 7c). The indicative characteristics of hopanes are listed in Table 3. The analyzed samples have Ts/Tm values of 0.15–1.00

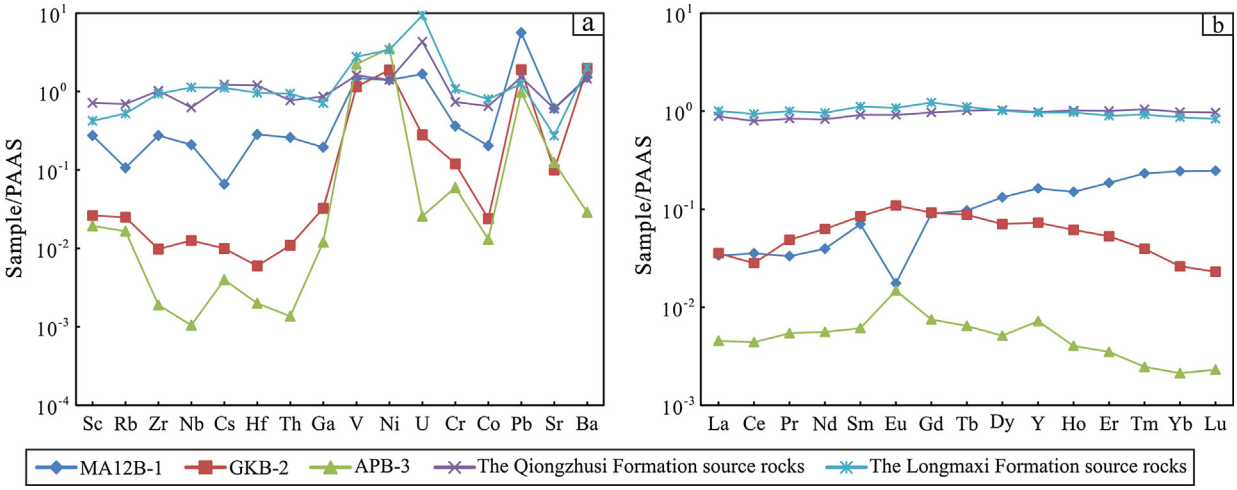

Fig. 8. PAAS-normalized trace elements in bitumen and possible source rocks showing: (a) relative abundances of trace elements and (b) relative abundances of REEs. Data for Longmaxi Formation source rocks were taken from Yan et al. (2009).

Table 6
REE compositions of the reservoir pure bitumen and PAAS.

Elements	Samples			
	PAAS	MA12B-1	GKB-2	APB-3
La (ppm)	38.2	1.29	1.36	0.174
Ce (ppm)	79.6	2.83	2.25	0.35
Pr (ppm)	8.83	0.294	0.43	0.048
Nd (ppm)	33.9	1.34	2.13	0.190
Sm (ppm)	5.55	0.39	0.47	0.034
Eu (ppm)	1.08	0.019	0.118	0.016
Gd (ppm)	4.66	0.42	0.43	0.035
Tb (ppm)	0.774	0.075	0.068	0.005
Dy (ppm)	4.68	0.62	0.33	0.024
Y (ppm)	27	4.4	1.97	0.195
Ho (ppm)	0.991	0.149	0.061	0.004
Er (ppm)	2.85	0.53	0.151	0.010
Tm (ppm)	0.405	0.094	0.016	0.001
Yb (ppm)	2.82	0.69	0.074	0.006
Lu (ppm)	0.433	0.107	0.010	0.001
REE + Y (ppm)	212	13.2	9.87	1.09
Y/Ho	27.3	29.5	32.3	48.8
Ce/Ce^*	1.00	1.06	0.68	0.88
Eu/Eu^*	1.00	0.22	1.24	2.18

(mean Ts/Tm = 0.56), C_{30} diahopane/C_{30} hopane = 0.04–0.14 (mean = 0.08), C_{29} 25-norhopane/C_{30} hopane = 0.04–0.07 (mean = 0.06), hopane C_{31} 22S/(22S + 22R) = 0.44–0.55 (mean = 0.51), and gammacerane/C_{30} hopane = 0.13–0.37 (mean = 0.18).

Terpane distributions in the Dengying samples are similar to those in the Longwangmiao samples (Table 3; Fig. 7f and g). C_{23} tricyclic terpane/C_{30} hopane = 0.10 to 0.15 (mean = 0.13), C_{24} tetracyclic terpane/(C_{24} tetracyclic terpane + C_{26} tricyclic terpane) = 0.33–0.43 (mean = 0.38), Ts/Tm = 0.70–1.01 (mean = 0.85), C_{30} diahopane/C_{30} hopane = 0.07–0.13 (mean = 0.10), C_{29}-25-norhopane/C_{30} hopane = 0.03–0.06 (mean = 0.04), hopane C_{31} 22S/(22S + 22R) = 0.54–0.55 (mean = 0.55), and gammacerane/C_{30} hopane = 0.09–0.29 (mean = 0.20). Thus, C_{26} tricyclic terpane/C_{25} tricyclic terpane, Ts/Tm, and gammacerane/C_{30} hopane are higher and C_{23} tricyclic terpane/C_{30} hopane ratios are lower in the Dengying samples relative to the Longwangmiao samples.

4.2.2.3. Steranes. Abundant steranes, e.g., C_{21} and C_{22} steranes, diasteranes, and C_{27}–C_{29} regular steranes (Fig. 7d; Table 4), were detected in the Longwangmiao samples. From these, the C_{29} ααα20R sterane is more abundant than the C_{27} ααα20R sterane in almost all the samples, with sterane C_{27} ααα20R/C_{29} ααα20R

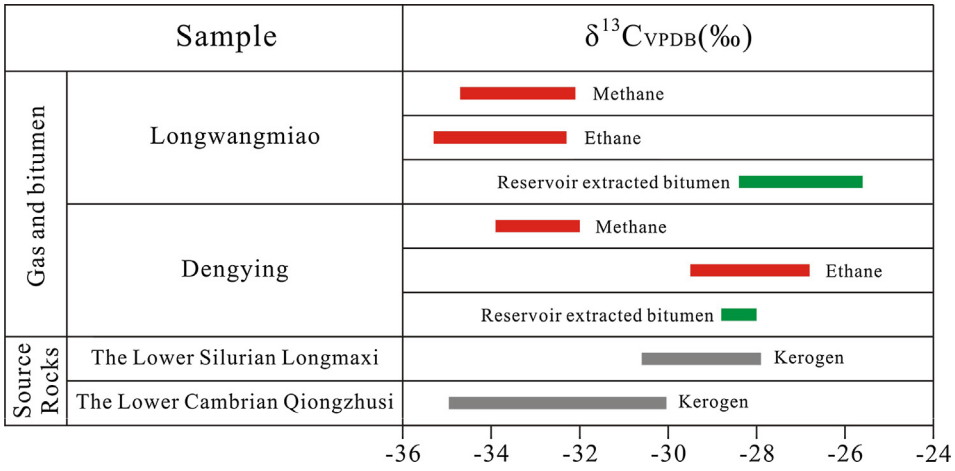

Fig. 9. Carbon isotope compositions of gas, bitumen, and possible source rocks (kerogen) from the Leshan–Longnvsi paleo-uplift area in the Sichuan Basin. Previously published values were taken from Liang et al. (2009), Liu et al. (2012), Wei et al. (2014, 2015) and Zou et al. (2014b).

= 0.58–1.01 (mean = 0.84; Table 4). Regular sterane/hopane = 0.23–0.73 (mean = 0.36), and diasterane/regular sterane = 0.23–0.43 (mean = 0.30). The parameters indicating maturity, sterane C_{29} ααα20S/(20S + 20R) and sterane C_{29} ββ/(αα + ββ), have values of 0.36–0.50 (mean = 0.46) and 0.34–0.45 (mean = 0.39), respectively.

Sterane distributions detected in the Dengying samples are similar to those in the Longwangmiao samples, but their ratios differ (Fig. 7h; Table 4). The Dengying samples contain more C_{29} ααα20R sterane than C_{27} ααα20R sterane, with sterane C_{27} ααα20R/C_{29} ααα20R = 0.58–0.80 (mean = 0.65). Regular sterane/hopane = 0.29–0.41 (mean = 0.37), diasterane/regular sterane = 0.18–0.35 (mean = 0.24), sterane C_{29} ααα20S/(20S + 20R) = 0.42–0.53 (mean = 0.47), and sterane C_{29} ββ/(αα + ββ) = 0.36–0.43 (mean = 0.39). Thus, %C_{29} ααα20R (sterane C_{29} ααα20R/(sterane C_{27} ααα20R + sterane C_{28} ααα20R + sterane C_{29} ααα20R) × 100%), and regular sterane/hopane are higher in Dengying samples, whereas sterane C_{27} ααα20R/C_{29} ααα20R, %C_{27} ααα20R (sterane C_{27} ααα20R/(sterane C_{27} ααα20R + sterane C_{28} ααα20R + sterane C_{29} ααα20R) × 100%), %C_{28} ααα20R (sterane C_{29} ααα20R/(sterane C_{27} ααα20R + sterane C_{28} ααα20R + sterane C_{29} ααα20R) × 100%), and diasterane/regular sterane are lower in Dengying samples, relative to Longwangmiao samples.

4.3. Trace element geochemistry

The total concentration of trace elements in the Longwangmiao reservoir bitumen is approximately 1666 ppm (Table 5), and Post-Archean Australian Shale (PAAS)-normalized trace element distributions are shown in Fig. 8a. It is showed that the Longwangmiao reservoir bitumen is relatively enriched in V, Ni, U, Pb, and Ba. In contrast, two samples from the Dengying Formation contain total trace element concentrations of 1647 and 606 ppm, which is a little different from that of the Longwangmiao samples (Table 5). The Dengying reservoir bitumen is enriched in V and Ni (Fig. 8a).

Rare earth element (REE) data are listed in Table 6. The total concentration of REEs in the Longwangmiao sample is approximately 13 ppm. The Longwangmiao reservoir bitumen shows a relative depletion in light REEs (LREEs) and enrichment in heavy REEs (HREEs; Fig. 8b). No Ce or Y element anomalies were observed, but a distinct negative Eu anomaly is evident. In contrast, two samples from the Dengying Formation show lower REE concentrations of 10

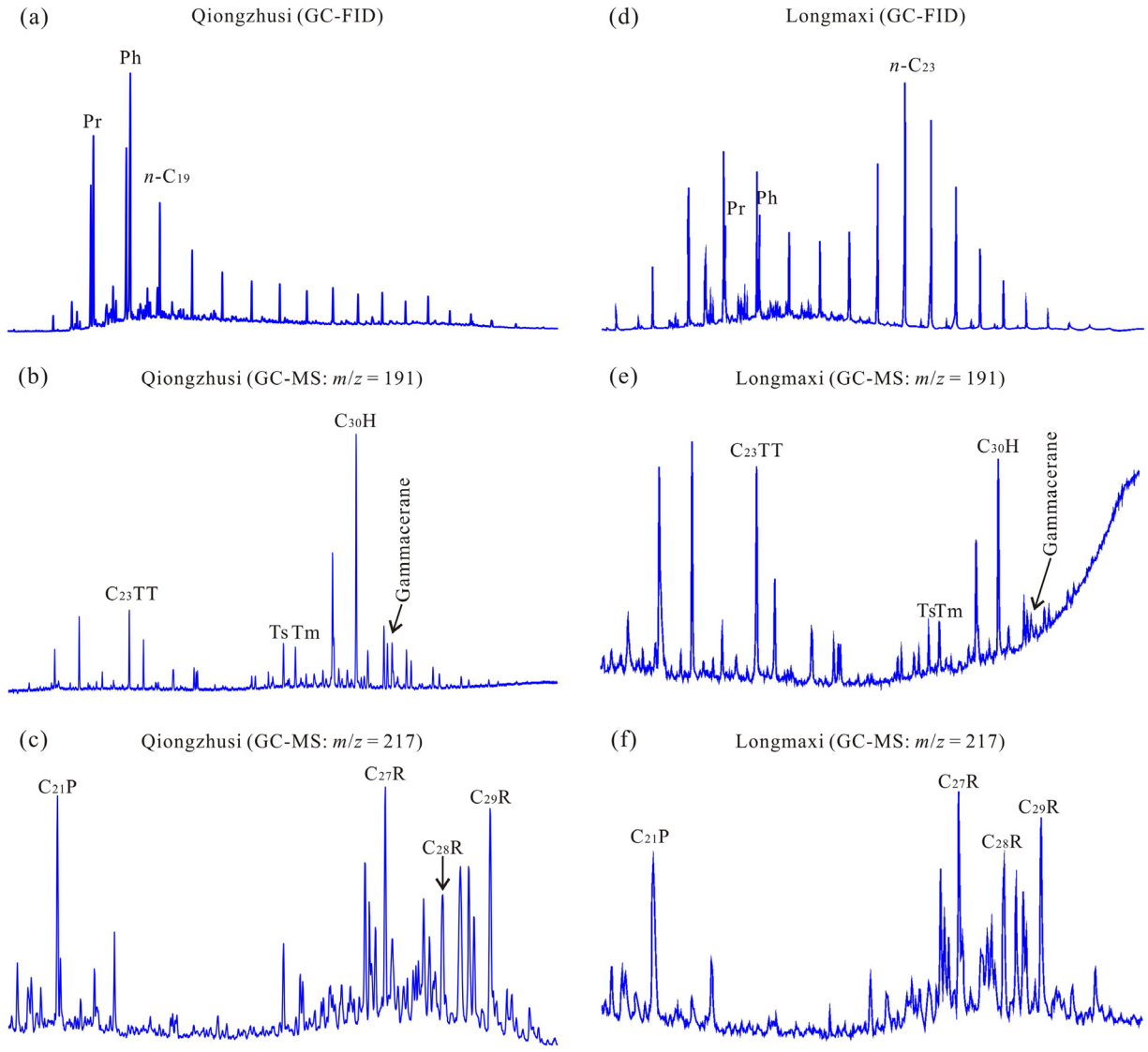

Fig. 10. GC-FID and GC–MS chromatograms of possible source rocks in the study area showing the (a–c) Qiongzhusi Formation (Liang et al., 2009) and (d–f) Longmaxi Formation (Li et al., 2013a). TT: tricyclic terpane; H: pentacyclic triterpane (hopane); Ts: 18α(H)-22,29,30-trinorhopane; Tm: 17α(H)-22,29,30-trinorhopane; P: C_{21} sterane; in (c) and (f) the 20R α,α,α-sterane isomers are labeled.

and 1 ppm, respectively. The REE patterns of the Dengying reservoir bitumen are nearly flat, with depleted heavy REEs. Besides, both samples show positive Eu and Y anomalies, with a negative Ce anomaly (Fig. 8b).

5. Discussion

5.1. Sources of bitumen

5.1.1. Insights from carbon isotopes

The stable carbon isotope signature of organic matter is an effective indicator of its source as it is typically only weakly affected by thermal or secondary effects (Stahl, 1977; Mazeas and Budzinski, 2002; Peters et al., 2005; Hoefs, 2008). Due to isotopic fractionation, the $\delta^{13}C$ of oil is approximately 1–2‰ lighter than its source kerogen (Galimov, 1985). Gas (especially $\delta^{13}C_2$) and residual bitumen formed by oil cracking are 1–2‰ lighter and 2–3‰ heavier, respectively, than their source oil (Machel et al., 1995). Therefore, the gas will be commonly 2–4‰ lighter and the residual bitumen 1–2‰ heavier than its source kerogen, and the extent of this fractionation depends on open or closed systems (Clayton, 1991; Rooney et al., 1995; Tang et al., 2000, 2005; Cai et al., 2006; Ni et al., 2011).

The variation of the Longwangmiao $\delta^{13}C$ values in this study is approximately 3‰ (Table 1; Section 4.2.1). We compared bitumen carbon isotopes with R_b to see whether maturity has an effect on the observed carbon isotope values. These results show no correlation ($r^2 = 0.01$, where r is the correlation coefficient). Therefore, we propose that the carbon isotope value of a bitumen is mainly a reflection of the source rock.

Fig. 9 shows the carbon isotope compositions of possible source rocks, reservoir bitumen and natural gas in the Longwangmiao and Dengying reservoirs. The ethane within the gas accumulations in the Gaoshiti–Moxi area (Longwangmiao) has $\delta^{13}C_2 = -35.3‰$ to $-32.3‰$ (Wei et al., 2014, 2015; Zou et al., 2014b), whereas the $\delta^{13}C$ value of reservoir bitumen in this area ranges from $-28.4‰$ to $-25.6‰$. Therefore, the $\delta^{13}C$ of the source kerogen of the Longwangmiao gas should range from $-33.3‰$ to $-26.6‰$. This value can be obtained by combining the Qiongzhusi and Longmaxi shales as source rocks.

In contrast, the ethane in gas accumulations and the reservoir bitumen in the Gaoshiti–Moxi area (Dengying) have carbon isotope values of $-29.5‰$ to $-26.8‰$ and $-28.8‰$ to $-28.0‰$, respectively, which differ significantly from those of the Longwangmiao reservoir. This may be caused by variability within the source rocks, given that the Dengying gas and bitumen were dominantly sourced from the Qiongzhusi Formation (Wei et al., 2013, 2014; Xu et al., 2014; Zheng et al., 2014).

5.1.2. Insights from alkanes, isoprenoids and biomarkers

5.1.2.1. Alkanes and isoprenoids. Saturated hydrocarbon chromatograms of *n*-alkanes from Longwangmiao extracted bitumen typically show one peak maximum at *n*-C_{19}–*n*-C_{22}, and a second population at *n*-C_{27} and C_{29}. In contrast, *n*-alkanes from Dengying extracted bitumen show one peak at *n*-C_{16}, *n*-C_{19}, and *n*-C_{20}.

n-Alkanes with a low carbon number are typically derived from algae, whereas higher carbon numbers are associated with terrestrial/terrigenous organisms (Peters et al., 2005 and references therein). However, pre-Silurian *n*-alkanes with high carbon numbers are not likely to have been derived from terrestrial/terrigenous organisms because there were no such organisms in the biosphere, and instead may have originated from a different source containing short-chain *n*-alkanes (Cranwell, 1977; Ficken et al., 2000). This would indicate that the two-peak distribution of *n*-alkanes likely originated from a mixed source (Tissot and Welte, 1984; Ebukanson and Kinghorn, 1986; Murray and Boreham, 1992), whereas the Dengying bitumen originated from a single source. The *n*-alkane composition in Qiongzhusi shales has one

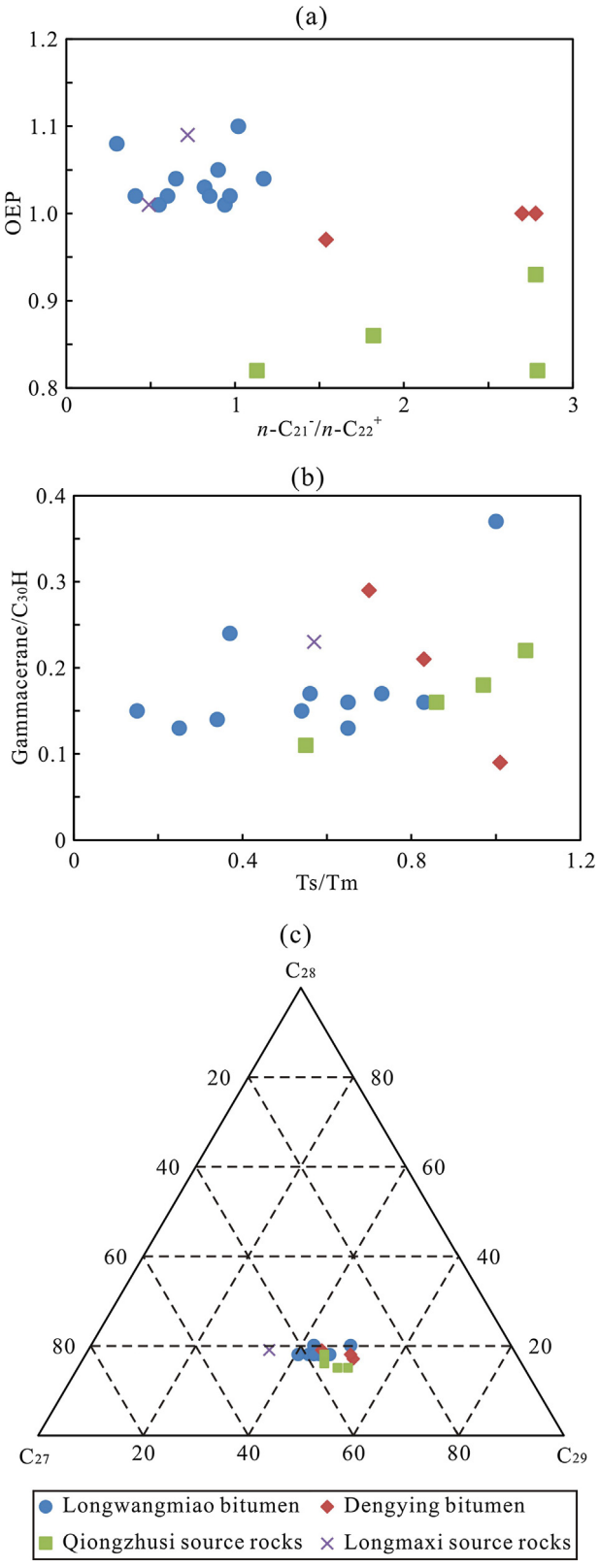

Fig. 11. Correlation of biomarker parameters of the Longwangmiao and Dengying bitumens and possible source rocks. Data of source rocks were taken from Ma et al. (2012), Tan et al. (2012), and Li et al. (2013a).

peak maximum at *n*-C_{18}, and in Longmaxi rocks has two peak maxima at *n*-C_{17} and *n*-C_{23} (Fig. 10; Li et al., 2013a). Thus, we infer that the Longwangmiao reservoir bitumen was derived from both the Qiongzhusi and the Longmaxi shales, and the bitumen of the Dengying reservoir was derived mainly from Qiongzhusi rocks. The correlation of OEP to $n\text{-}C_{21}^{-}/n\text{-}C_{22}^{+}$ shows that the Dengying reservoir bitumens are close to Qiongzhusi shales, while the Longwangmiao reservoir bitumens have more inclination towards Longmaxi source rocks (Fig. 11a), further supporting the interpretation above.

5.1.2.2. Terpanes. Saturated hydrocarbon mass chromatograms (m/z = 191) of Longwangmiao and Dengying bitumens show that the distribution of terpanes is generally similar in the two reservoirs (Fig. 7b and f). However, the ratios of individual terpanes show variation, implying different bitumen sources (Table 3). Typical parameters display that the bitumens plot generally in the shale region (Fig. 12). This suggests that both Longwangmiao and Dengying bitumens were sourced from shales, corresponding to the Qiongzhusi Formation. However, the Longwangmiao bitumens may have been partly sourced from carbonate rocks (Fig. 12), corresponding to interlayered carbonates in the Longmaxi Formation (Shen, 2014).

The Ts/Tm ratio also shows variation: 0.15–1.00 for Longwangmiao (mean = 0.56), and 0.70–1.01 for Dengying (mean = 0.85). This ratio is influenced by multiple and complex factors, such as source, depositional environment and thermal maturity of organic matter (Peters et al., 2005). Ts is typically associated with catalysis by clay minerals in clastic rocks under acidic environments; in addition, Ts is usually more thermally stable than Tm, which results in an increase in Ts/Tm with greater thermal maturity (Seifert and Moldowan, 1979; Moldowan et al., 1985). Note that all bitumens in this study are mainly of high maturity, thus the maturity may not be the main cause for the variabilities of Ts/Tm. Therefore, we infer that the source of the Longwangmiao bitumen is rocks with more carbonates than that of Dengying, and the maturity of the Longwangmiao bitumen is lower than the Dengying bitumen. This further supports the understanding obtained from petrology (Section 4.1) and alkane and terpane results above (Sections 5.1.2.1 and 5.1.2.2).

The gammacerane/C_{30} hopane ratio of the Longwangmiao bitumen ranges from 0.13 to 0.37 (mean = 0.18), while that of the Dengying bitumen is 0.09–0.29 (mean = 0.20). This suggests that both the bitumens are derived from organic matter deposited in relatively highly saline environments, corresponding to the known conclusions for the Qiongzhusi and Longmaxi shales. Correlation of Ts/Tm to gammacerane/C_{30} hopane ratios shows that the Longwangmiao bitumens are derived from both the Qiongzhusi and Longmaxi source rocks and the Dengying bitumen is derived mainly from the Qiongzhusi rocks (Fig. 11b).

5.1.2.3. Steranes C_{27}, C_{28} and C_{29}. Steranes show significant variability between the Longwangmiao and Dengying reservoir bitumens (Fig. 7d and h). For example, in the Longwangmiao reservoir, sterane C_{27} ααα20R/C_{29} ααα20R = 0.58–1.01 (mean = 0.84), and in the Dengying reservoir, sterane C_{27} ααα20R/C_{29} ααα20R = 0.58–0.80 (mean = 0.65). Huang and Meinschein (1979) proposed that sterane C_{27} and sterane C_{29} were derived from sterol C_{27} in lower organisms (some bacteria and algae), and sterol C_{29} in higher organisms (higher plants). However, steranes identified in organic matter from pre-Silurian sources that lack higher plants, indicates the complexity of the organism present (Dutta et al., 2013). Schwark and Empt (2006) proposed that the C_{27} sterane is sourced from red algae, and the C_{29} sterane from green algae (Volkman et al., 1999).

To evaluate the source contribution to the bitumens, we plotted relative composition of the C_{27}, C_{28} and C_{29} steranes (Fig. 11c), and this shows a characteristically low C_{28} abundance. This implies that the Longwangmiao bitumens are derived from both the Qiongzhusi and Longmaxi source rocks and the Dengying bitumens are derived dominantly from the Qiongzhusi rocks.

5.1.3. Insights from trace and rare earth elements

Trace elements can be used as indicators of the origin and accumulation history of bitumen and oils (Hirner, 1987; López et al., 1998; Alberdi-Genolet and Tocco, 1999; Galarraga et al., 2008; Shi et al., 2015). Oil and gas formation and evolution are influenced by complex organic–inorganic interactions (Tissot and Welte, 1984). Therefore, inorganic components are present in oils, reservoir extractions and bitumens (Barwise, 1990; Filby, 1994; Alberdi-Genolet and Tocco, 1999; Akinlua et al., 2007; Galarraga et al., 2008). Furthermore, the relative concentrations of some trace elements, such as V, Ni, and REEs, may be indicative of organic facies since they are nearly unaffected by hydrocarbon migration, and are generally resistant to hydrocarbon maturity and secondary alteration (Lewan, 1984; Hunt, 1996; Quinby-Hunt and Wilde, 1996; Wilde et al., 2004; Galarraga et al., 2008).

The V/Ni, also presented as V/(V + Ni) ratios, is the most widely used elemental parameter in hydrocarbon–source correlations, because these ratios vary significantly between different sedimentary settings and are typically not influenced by reservoir mineralogy or fluid migration (Lewan, 1980; Karlsen et al., 1995; López

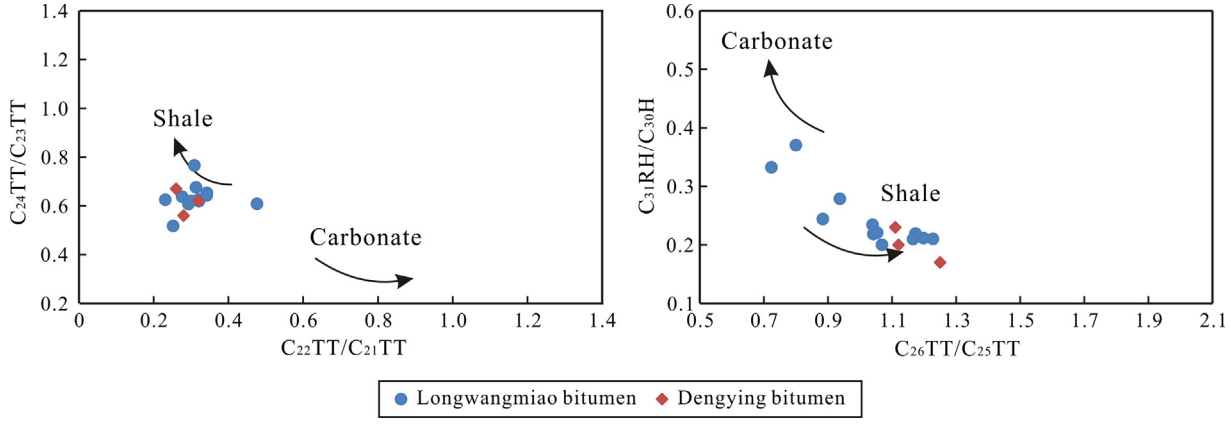

Fig. 12. Correlation of terpane parameters in the Longwangmiao and Dengying bitumens. TT: tricyclic terpane; H: pentacyclic triterpane (hopane); RH: 20R hopane. The distinguishing standards are after Peters et al. (2005) and Al-Ameri and Zumberge (2012).

et al., 1998; López and Lo Mónaco, 2004). In this study, source rocks of bitumen are dominantly marine shales. Thus, there is enough SO_4^{2-} in seawater and associated shales, and NiS will deposit under favorable pH and Eh conditions. This warrants the generally effective application of the ratios V/Ni and V/(V + Ni) (Karlsen et al., 1995). Studies have shown that bitumen derived from source rocks deposited in an euxinic environment yield V/(V + Ni) > 0.84, whereas bitumen derived from anoxic sediments yields V/(V + Ni) = 0.54–0.84, and bitumen derived from dysoxic source rocks yields V/(V + Ni) = 0.46–0.60 (Hatch and Leventhal, 1992). The V/(V + Ni) value of the Longwangmiao bitumen is 0.74, indicating that it was derived from source rocks deposited in a lacustrine anoxic environment, while the V/(V + Ni) value of Dengying bitumen ranges from 0.62 to 0.63 (mean = 0.63), suggesting that it was derived from source rocks deposited in a marine anoxic environment.

The Ni/Co values of organic matter can be used to identify the depositional environment of the source rocks. For example, Jones and Manning (1994) compared the Ni/Co ratios and degree of pyritization (DOP) of shales, and proposed that a Ni/Co ratio of > 7.0 is

Table 7
Geochemical parameters of the Longwangmiao and Dengying gases in the Gaoshiti–Moxi area of the Sichuan Basin. Data were taken from Wei et al. (2014, 2015) and Zou et al. (2014b).

Reservoir	Well	Composition (%)			Gas dryness	Carbon isotopes (‰)		Reference
		CH_4	C_2H_6	C_3H_8		$\delta^{13}C_1$	$\delta^{13}C_2$	
Longwangmiao	Moxi 8	96.80	0.14	/	1.00	−32.4	−32.3	Wei et al. (2014)
		96.85	0.14	/	1.00	−33.1	−33.6	Wei et al. (2014)
		96.81	0.14	0.009	1.00	−32.5	−32.4	Zou et al. (2014b)
		96.84	0.14	0.010	1.00	−33.2	−33.7	Zou et al. (2014b)
	Moxi 9	95.16	0.13	/	1.00	−32.8	−32.8	Wei et al. (2014)
		95.15	0.13	0.007	1.00	−32.9	−32.8	Zou et al. (2014b)
	Moxi 10	97.35	0.13	/	1.00	−32.1	−33.6	Wei et al. (2014)
	Moxi 11	97.09	0.13	/	1.00	−32.5	−32.4	Wei et al. (2014)
		97.12	0.13	/	1.00	−32.6	−32.5	Wei et al. (2014)
		97.08	0.13	0.005	1.00	−32.5	−32.4	Zou et al. (2014b)
		97.11	0.13	0.004	1.00	−32.6	−32.5	Zou et al. (2014b)
	Moxi 13	95.44	0.13	/	1.00	−32.7	−33.0	Wei et al. (2015)
	Moxi 16	96.16	0.14	/	1.00	−32.5	−32.7	Wei et al. (2015)
	Moxi 17	95.24	0.14	/	1.00	−32.7	−34.1	Wei et al. (2015)
	Moxi 21	95.21	0.27	/	1.00	−33.5	−34.9	Wei et al. (2015)
	Moxi 201	95.91	0.13	/	1.00	−33.1	−33.0	Wei et al. (2015)
	Moxi 202	95.48	0.15	/	1.00	−34.7	−35.3	Wei et al. (2015)
	Moxi 204	96.63	0.13	/	1.00	−32.6	−32.4	Wei et al. (2015)
	Moxi 205	95.30	0.20	/	1.00	−33.2	−34.8	Wei et al. (2015)
	Moxi 008-H1	95.15	0.14	/	1.00	−32.2	−33.3	Wei et al. (2015)
	Moxi 009-X1	96.50	0.14	/	1.00	−33.0	−33.3	Wei et al. (2015)
Dengying	Gaoshi 1	91.22	0.04	/	1.00	−32.3	−28.1	Wei et al. (2014)
		90.11	0.04	/	1.00	−32.7	−28.4	Wei et al. (2014)
		82.65	0.04	/	1.00	−32.3	−27.8	Wei et al. (2014)
		90.12	0.04	0.002	1.00	−32.6	−28.5	Zou et al. (2014b)
		82.66	0.04	0.001	1.00	−32.2	−28.8	Zou et al. (2014b)
	Gaoshi 2	92.14	0.04	/	1.00	−33.1	−27.6	Wei et al. (2014)
	Gaoshi 3	90.19	0.04	/	1.00	−33.1	−28.1	Wei et al. (2014)
		86.62	0.03	/	1.00	−32.6	−28.0	Wei et al. (2014)
		90.18	0.04	0.001	1.00	−33.2	−28.2	Zou et al. (2014b)
	Gaoshi 6	90.12	0.04	/	1.00	−33.0	−27.8	Wei et al. (2014)
		90.29	0.04	/	1.00	−32.9	−28.6	Wei et al. (2014)
		94.61	0.04	/	1.00	−32.8	−29.1	Wei et al. (2014)
		89.97	0.04	0.001	1.00	−32.8	−28.7	Zou et al. (2014b)
		94.60	0.05	0.002	1.00	−32.8	−29.1	Zou et al. (2014b)
	Gaoshi 8	92.49	0.03	/	1.00	−32.8	−27.7	Wei et al. (2015)
		91.49	0.04	/	1.00	−33.2	−28.8	Wei et al. (2015)
	Gaoshi 9	89.63	0.03	/	1.00	−33.5	−28.1	Wei et al. (2015)
		91.71	0.03	/	1.00	−33.5	−27.7	Wei et al. (2015)
		91.21	0.03	/	1.00	−33.6	−27.3	Wei et al. (2015)
	Gaoshi 10	90.04	0.03	/	1.00	−33.4	−28.2	Wei et al. (2015)
		91.37	0.03	/	1.00	−33.4	−27.6	Wei et al. (2015)
	Moxi 8	91.40	0.04	/	1.00	−32.8	−28.3	Wei et al. (2014)
		91.42	0.04	/	1.00	−32.3	−27.5	Wei et al. (2014)
		91.41	0.03	0.001	1.00	−32.9	−28.4	Zou et al. (2014b)
		91.43	0.04	0.001	1.00	−32.2	−27.4	Zou et al. (2014b)
	Moxi 9	91.82	0.05	/	1.00	−33.5	−28.8	Wei et al. (2014)
		91.81	0.05	0.001	1.00	−33.4	−28.7	Zou et al. (2014b)
	Moxi 10	93.13	0.05	/	1.00	−33.9	−27.8	Wei et al. (2014)
		93.12	0.05	0.002	1.00	−33.9	−27.8	Zou et al. (2014b)
	Moxi 11	92.75	0.05	/	1.00	−33.9	−27.6	Wei et al. (2014)
		89.87	0.03	/	1.00	−32.0	−26.8	Wei et al. (2014)
		89.88	0.03	0.001	1.00	−32.1	−26.9	Zou et al. (2014b)
	Moxi 12	92.76	0.04	/	1.00	−33.1	−29.3	Wei et al. (2015)
	Moxi 13	90.47	0.04	/	1.00	−32.9	−29.5	Wei et al. (2015)
	Moxi 17	92.45	0.03	/	1.00	−33.5	−28.9	Wei et al. (2015)
		89.88	0.04	/	1.00	−33.3	−27.5	Wei et al. (2015)

Note: "/" denotes value below detection limits.

characteristic of an anoxic environment, whereas Ni/Co = 5.0–7.0 is typical of dysoxic environments. The Ni/Co value of Longwangmiao bitumen is 16.4, indicating that its source rocks were deposited in an anoxic environment. Dengying reservoir bitumen yields Ni/Co = 189–657 (mean Ni/Co = 423), indicating that the environment of deposition of its source rocks was significantly more anoxic than that of the inferred Longwangmiao source rocks.

The V/Cr values of organic matter can also be used as an indicator of the depositional environment of the source rocks. Jones and Manning (1994) compared V/Cr ratios and the degree of pyritization (DOP) of shales, showing that Ni/Co > 4.25 is typical of anoxic deposition, Ni/Co = 2.00–4.25 is characteristic of dysoxic deposition. The V/Cr value of Longwangmiao bitumen is 5.6, whereas Dengying bitumen has V/Cr = 13–51 (mean V/Cr = 32). Therefore, both bitumens were derived from source rocks deposited in anoxic environments.

The U/Th values of organic matter can also be used as an indicator of the depositional environment of the source rocks. Jones and Manning (1994) compared U/Th ratios and the degree of pyritization (DOP) of shales, and found that U/Th > 1.25 is typical of anoxic deposition, Ni/Co = 0.75–1.25 is characteristic of dysoxic deposition. In this study, the U/Th value of Longwangmiao bitumen is 1.4, whereas Dengying bitumen has U/Th = 4.0–5.4 (mean U/Th = 4.7). Therefore, both bitumens were derived from source rocks deposited under anoxic environments.

In consideration of all the four trace element ratios above, we infer that both the Longwangmiao and Dengying bitumens are derived from source rocks deposited in anoxic environments and that of the Dengying bitumen is relatively more anoxic than that of the Longwangmiao bitumen. Studies have shown that the Qiongzhusi rocks were deposited in a more anoxic environment than the Longmaxi rocks (Yan et al., 2009; Li et al., 2013b). Therefore, the Longwangmiao bitumen was contributed by mixing of more anoxic Qiongzhusi rocks with less anoxic Longmaxi rocks, whereas the Dengying bitumen was mainly derived from the anoxic sediments of the Qiongzhusi Formation. Still, note that the pH and Eh conditions of the depositional environment have complex influences on these ratios, which are not known sufficiently. Thus, these ratios should be used in the context of geology and combined with other evidence. The integrated discussion above warrants a plausible first model.

The REE patterns in Longwangmiao bitumen show a relative depletion in LREEs, enrichment in HREEs, a negative Eu anomaly, and no Ce or Y anomalies (Fig. 8b). In contrast, REEs in Dengying bitumen show mountain-type REE patterns with positive Eu anomalies, negative Ce and positive Y anomalies (Fig. 8b). In comparison, the Qiongzhusi shale does not have a negative Eu anomaly, but the Longmaxi shale has a small negative Eu anomaly. Thus, the Eu anomaly in Longwangmiao bitumen may reflect mixed Qiongzhusi and Longmaxi sources. In contrast, the REE patterns of Dengying bitumen are dominantly controlled by the Qiongzhusi shale.

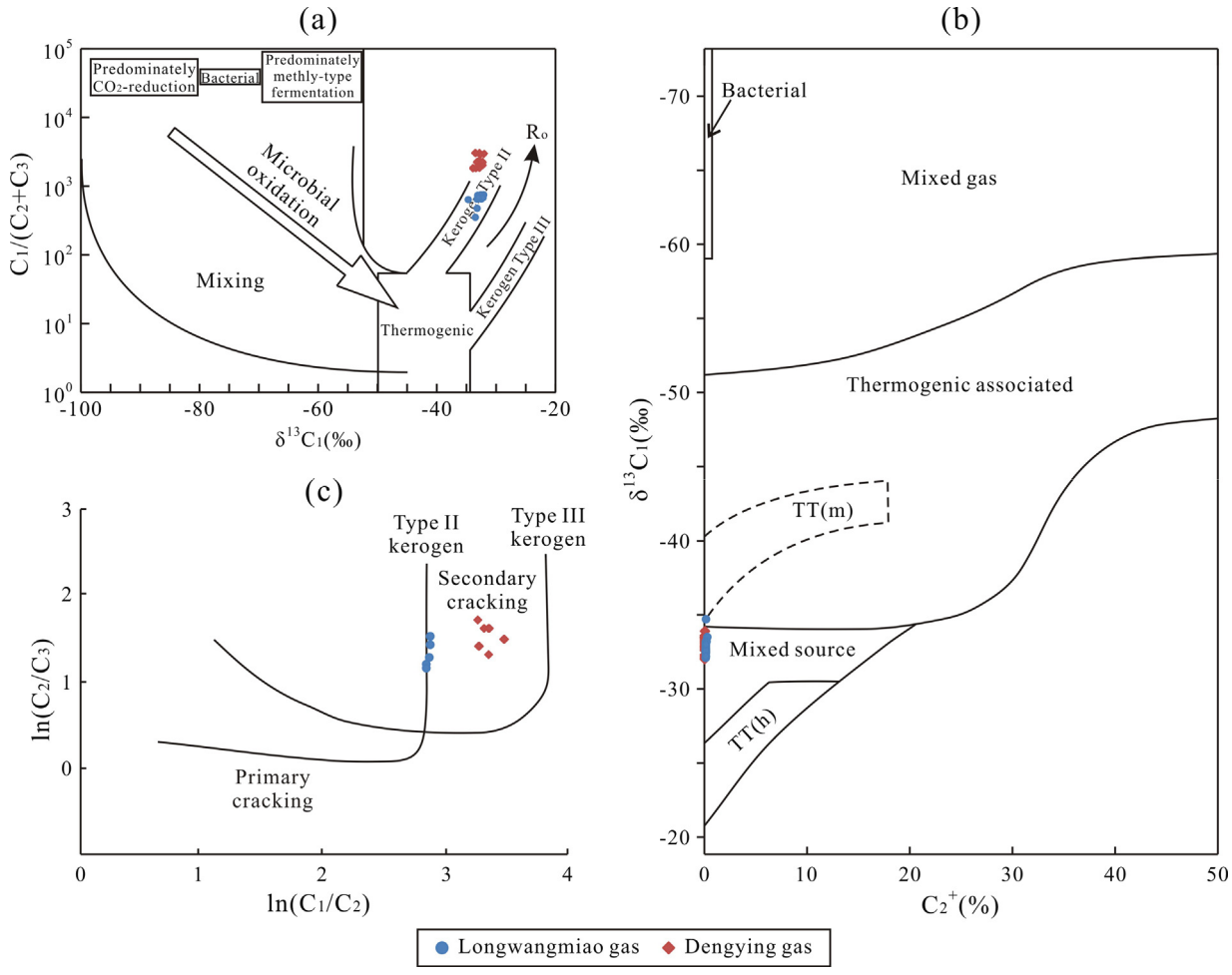

Fig. 13. Natural gas geochemistry showing gas origin: (a) Bernard diagram to delineate gas genetic types (Bernard et al., 1978; Faber and Stahl, 1984; Whiticar, 1996); (b) relative concentration of gas components in relation to stable carbon isotope composition of methane (Schoell, 1983); mixed gas: mixing of thermogenic and bacterial gas; TT (m): non-associated dry gases from sapropelic liptinic organic matter; TT (h): non-associated gases from humic organic matter; Mixed source: mixed of TT (m) and TT (h); (c) Molecular proportions C_2/C_3 versus C_1/C_2 in gas, in logarithmic scales (Behar et al., 1991).

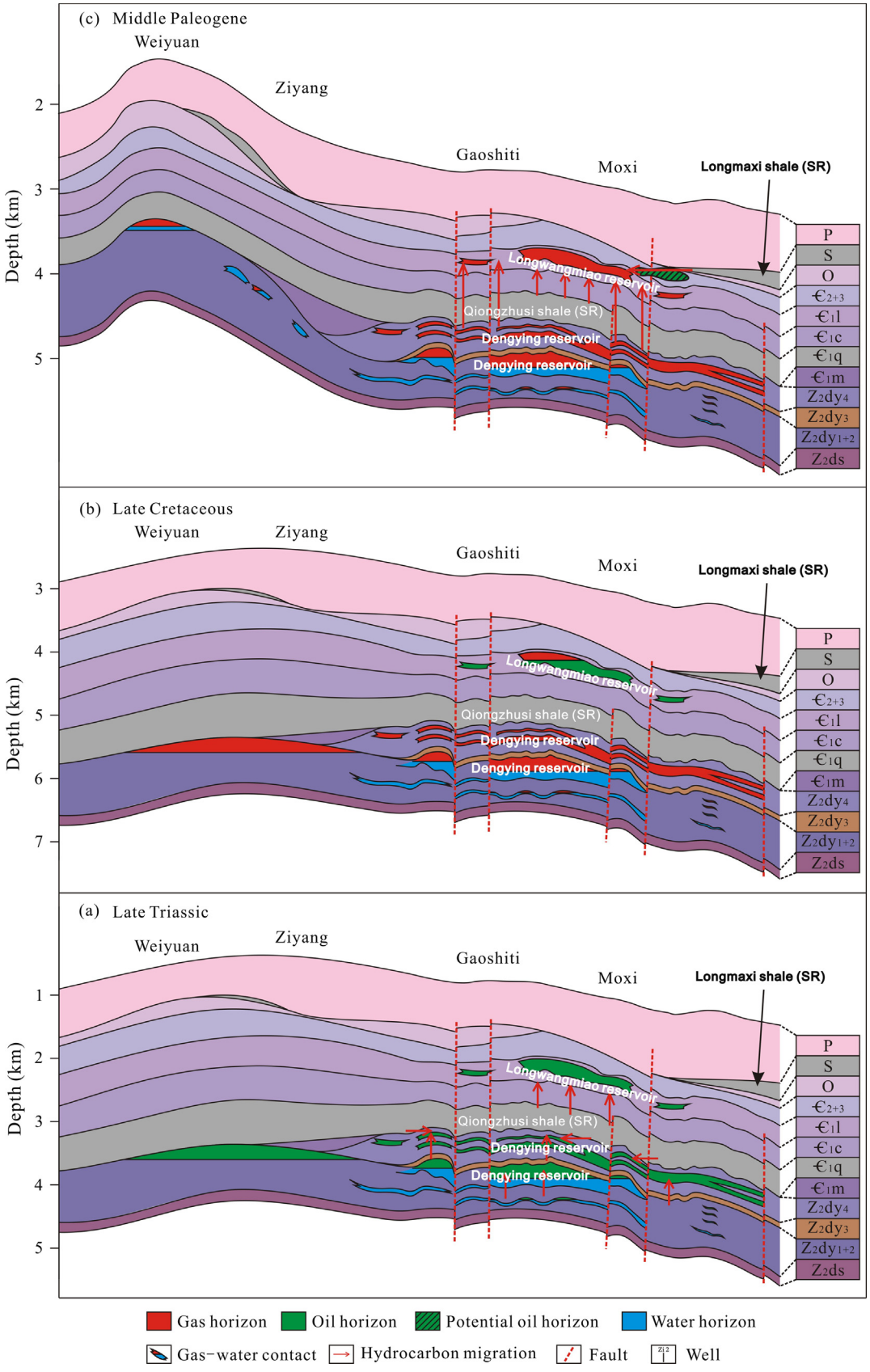

Fig. 14. Model of oil–gas charging and gas accumulation in the Lower Cambrian Longwangmiao and Sinian Dengying reservoirs, Sichuan Basin. See Fig. 3 for the meaning of the letters.

In summary, we conclude that the Longwangmiao bitumen was derived dominantly from the Qiongzhusi Formation (Type A solid bitumen), with a relatively minor component being derived from the Longmaxi Formation (Type B oil bitumen). This contrasts with Dengying bitumen, which was derived dominantly from the Qiongzhusi Formation.

5.2. Origin of natural gas

The natural gas composition and stable isotopes have been widely used in the identification of natural gas origins. In this study, C_1 and C_2 compositions and stable isotopes were collected because the gas is extremely dry and thus relatively higher homologs (e.g., C_3 and C_4) could not always be detected. We plotted these values (Table 7) in traditional Schoell and Whiticar diagrams (Fig. 13a and b). Results suggested that both the Longwangmiao and Dengying gases are mainly sourced from sapropelic organic matter with Type II kerogen and are highly mature. The Dengying gases are slightly more mature than the Longwangmiao gases. In the Prinzhofer diagram (Fig. 13c), both gases are suggested to originate from oil-cracking from Type II kerogen, consistent with the understanding obtained above. These characteristics indicate that the Longwangmiao and Dengying gases are have the same oil-cracking origin and the Dengying gas is relatively more mature. However, the reservoir temperature excludes the possibility of in situ oil-cracking in the Longwangmiao reservoir, whereas it is possible in the Dengying reservoir (Fig. 5). Thus, we infer that the Longwangmiao gas accumulation is the result of a later migration from a deep-sited Dengying gas accumulation. Additional evidence for his remigration model is that the Dengying gases are drier and more mature than the Longwangmiao gases. This may be caused by fractionation during the remigration in that less mature gas migrate upward to shallower reservoirs while more mature gas accumulated downward in deeper reservoirs. Second, the difference of $\delta^{13}C_2$ between the Longwangmiao and Dengying gases may be caused by Rayleigh fractionation (Rayleigh, 1896; Galimov, 1988; Clayton, 1991; Rooney et al., 1995; Wu et al., 2016), which results in the variation of gas $\delta^{13}C_2$ along with the increasing of reservoir temperature.

5.3. Accumulation process of the Longwangmiao reservoir

Combining all the results and understanding above and based on the geology, we can reconstruct the accumulation process of the Longwangmiao reservoir (Fig. 14). During the Late Triassic of the Indosinian Epoch, the Lower Cambrian Qiongzhusi source rocks reached the peak for petroleum generation. Oils migrated into both the shallower Longwangmiao and deeper Dengying reservoirs, forming paleo-reservoirs (Fig. 14a).

Subsequently, since the Late Cretaceous of the Yanshanian Epoch, the Dengying reservoir has reached the threshold for oil cracking (Fig. 5) and oils started to crack to gas (Fig. 14b). This is the second critical moment for gas formation. Pyrobitumen is the other end-member product of this process (Fig. 6e and f). In contrast, the Longwangmiao reservoir had not reached the threshold for oil cracking as outlined above (Fig. 5). In addition, within carbonates like the Longwangmiao, oil is much more stable at high temperatures than in shales/siliclastic reservoirs because carbonate is inert with respect to oil; therefore, there was mainly oil with a little gas in the Longwangmiao reservoir at this stage.

Later, during the Cenozoic, under the influence of the Himalaya movement, there is common uplifting and fault activities in the study area (Li et al., 2014a). As a consequence, gas in the deeper Dengying reservoir remigrated into the shallower Longwangmiao reservoir along faults (c.f., Karlsen and Skeie, 2006; Lerch et al., 2016). Meanwhile, the Qiongzhusi source rocks reached the dry gas window, and thus kerogen-cracking gas also charged into the Longwangmiao reservoir (Fig. 14c). Gas gravity drainage and phase separation took place, resulting in the formation of solid bitumen (Type A bitumen; Fig. 6a–d) and the saturated fraction of the extracted reservoir bitumen being lack of light-end *n*-alkanes (Fig. 10). Note that this remigration might not be the classic Silverman/Gussow type remigration (Silverman, 1965; Gussow, 1968) because there is no series of traps along the updip-downdip direction, and the reservoirs are currently dominated by gas with little oil.

After this gas remigration, oil generated from the Longmaxi source rocks migrated into the Longwangmiao reservoir (Fig. 14c), forming the Type B oil bitumen in the Longwangmiao reservoir (Fig. 6c and d). The oil generated by the Longmaxi shales passed through several Middle–Upper Cambrian lithological units during its migration into the Longwangmiao reservoir. Note that because of the structural uplifting and fault activity, the Longwangmiao reservoir oils may have been subjected to biodegradation to varying degrees (c.f., Ohm et al., 2012) and leakage (c.f., Magoon and Dow, 1994). Thus, 25-norhopanes indicative of hydrocarbon biodegradation were detected (Table 3; Fig. 7d) and light-end *n*-alkanes have a relatively low abundance (Fig. 7a).

Note that both the Dengying and the Longwangmiao reservoirs have relatively good preservation conditions for hydrocarbon. The Longwangmiao intercalated evaporites and mudstones of the Middle Cambrian Gaotai Formation and Permian act as high quality cap rocks for the Longwangmiao gas (Fig. 2). For the Dengying gas, there is an additional source rock candidate, i.e., the Lower Cambrian Qiongzhusi shales (Fig. 2). Thus, the hydrocarbon preservation potential for these "super old" gas systems is relatively good, favoring the formation of giant gas reservoirs despite the gas loss during their long geological evolution (Tissot and Welte, 1984; Magoon and Dow, 1994).

Therefore, the petroleum migration and accumulation pattern for the Longmaxi reservoir in the study area is complex, and possibly somewhat non-traditional, i.e., lateral migration from deep-sited and younger Longmaxi source rocks in sags to shallow-sited and older Longwangmiao dolomite reservoirs in uplifts. In this view, we propose that future exploration projects should include investigations of both the oil- and gas-producing potential of the Longmaxi Formation, because the thermal maturity of the Longmaxi shales is approximately 1.3 %Ro and both oil and gas are expected to be generated. Furthermore, based on the new model presented in this paper (Fig. 14), we suggest that Middle–Upper Cambrian and Ordovician reservoirs, particularly along the top of the Cambrian successions, might be good exploration targets for primary oil.

6. Conclusions

The origins of bitumen in the Lower Cambrian Longwangmiao reservoir of the Moxi and Gaoshiti areas, Sichuan Basin, are complex. The Longwangmiao bitumen contains highly mature solid bitumen and a newly identified oil bitumen of low maturity; this differs from that in the Dengying reservoir, which only contains highly mature solid bitumen.

High maturity solid bitumen and low maturity oil bitumen in the Longwangmiao Formation were possibly derived from the shales of the Lower Cambrian Qiongzhusi and Silurian Longmaxi formations, respectively, but it is still not clear why the $\delta^{13}C$ of bitumen is enriched or equal to the proposed source rocks samples. This needs further study.

Petroleum generated from the Qiongzhusi Formation migrated into the Longwangmiao and Dengying reservoirs during the Indosinian Epoch, forming paleo-reservoirs. Later, the Dengying oil cracking had started since the Late Cretaceous, which is the critical moment for the gas. Following this, during the Himalayan Epoch

(the Cenozoic), the gas in the Dengying reservoir, together with kerogen-cracking gas from the Qiongzhusi source rocks, migrated into the Longwangmiao reservoir along faults. Gas washing on oils took place and solid bitumen was formed. Later, the oil generated from the Longmaxi shales migrated into the Longwangmiao reservoir. This resulted in the existence of both solid bitumen and oil bitumen in the reservoir.

Future exploration targets should include both oil and gas in the Longmaxi source rocks, and Upper Cambrian reservoirs along the top of Cambrian strata.

Acknowledgements

We thank Dr. Dariusz Strąpoć, Prof. Dr. Dag Karlsen, and the other two anonymous reviewers for their constructive and detailed reviews, which significantly improved the article. Editor-in-Chief John Volkman is thanked for kindly handling this manuscript. We thank the technical staffs from the Research Institute of Exploration and Development of PetroChina Southwest Oil & Gas Field Company for their assistance in completing the work. This work was jointly funded by the National Science and Technology Major Project of China (Grant No. 2016ZX05004-002-001) and National Natural Science Foundation of China (Grant Nos. 41322017 and 41472100).

Associate Editor—**Dariusz Strąpoć**

References

Akinlua, A., Ajayi, T.R., Adeleke, B.B., 2007. Organic and inorganic geochemistry of Northwestern Niger Delta. Geochemical Journal 41, 271–281.
Akinlua, A., Sigedle, A., Buthelezi, T., Fadipe, O.A., 2015. Trace element geochemistry of crude oils and condensates from South African Basins. Marine and Petroleum Geology 59, 286–293.
Akinlua, A., Torto, N., Ajayi, T.R., 2008. Determination of rare earth elements in Niger Delta crude oils by inductively coupled plasma-mass spectrometry. Fuel 87, 1469–1477.
Al-Ameri, T.K., Zumberge, J., 2012. Middle and Upper Jurassic hydrocarbon potential of the Zagross Fold Belt, North Iraq. Marine and Petroleum Geology 36, 13–34.
Alberdi-Genolet, M., Tocco, R., 1999. Trace metals and organic geochemistry of the Machiques Member (Aptian–Albian) and La Luna Formation (Cenomanian–Campanian), Venezuela. Chemical Geology 160, 19–38.
Barwise, A.J., 1990. Role of nickel and vanadium in petroleum classification. Energy & Fuels 4, 647–652.
Behar, F., Ungerer, P., Kressmann, S., Rudkiewicz, J.L., 1991. Thermal evolution of crude oils in sedimentary basins: experimental simulation in a confined system and kinetic modeling. Revue de l'Institut français du pétrole 46, 151–181.
Bernard, B.B., Brooks, J.M., Sackett, W.M., 1978. Light hydrocarbons in recent Texas continental shelf and slope sediments. Journal of Geophysical Research: Oceans 83, 4053–4061.
Bureau of Geology and Mineral Resources of Sichuan Province, 1991. Regional Geology of Sichuan Province. Geological Publishing House, Beijing (in Chinese).
Cai, X.Y., Zhu, Y.M., Huang, R.C., 2006. Geochemical behaviors and origin of reservoir bitumen in Puguang gas pool. Oil and Gas Geology 27, 340–347 (in Chinese with English abstract).
Carminati, E., Cavazza, D., Scrocca, D., Fantoni, R., Scotti, P., Doglioni, C., 2010. Thermal and tectonic evolution of the southern Alps (northern Italy) rifting: coupled organic matter maturity analysis and thermokinematic modeling. American Association of Petroleum Geologists Bulletin 94, 369–397.
Cheng, K.M., Wang, S.Q., Dong, D.Z., Huang, J.L., Li, X.J., 2009. Accumulation conditions of shale gas reservoirs in the Lower Cambrian Qiongzhusi Formation, the Upper Yangtze region. Natural Gas Industry 29, 40–44 (in Chinese with English abstract).
Clayton, C., 1991. Carbon isotope fractionation during natural gas generation from kerogen. Marine and Petroleum Geology 8, 232–240.
Cranwell, P.A., 1977. Organic geochemistry of Cam Loch (Sutherland) sediments. Chemical Geology 20, 205–221.
Dai, J.X., 2003. Pool-forming periods and gas sources of Weiyuan gasfield. Petroleum Geology & Experiment 25, 473–480 (in Chinese with English abstract).
Dai, J.X., Wang, T.D., Dai, H.M., Xia, X.Y., Zhao, M.J., 2000. The gas resource of the great gas field in carbonate rocks in China (Abstract). Marine Origin Petroleum Geology 5, 12–13 (in Chinese).
Deng, K.L., 1992. Formation and evolution of Sichuan Basin and domains for oil and gas exploration. Natural Gas Industry 12, 7–12 (in Chinese with English abstract).
Du, J.G., Wang, C.Y., Wang, W.C., Cui, Y.J., Zhang, W.B., 2012. Effects of high pressure and temperature on carbon isotope compositions of some acyclic alkanes and preservation of organic matter. High Pressure Research 32, 220–232.
Dutta, S., Bhattacharya, S., Raju, S.V., 2013. Biomarker signatures from Neoproterozoic–early Cambrian oil, western India. Organic Geochemistry 56, 68–80.
Ebukanson, E.J., Kinghorn, R.R.F., 1986. Maturity of organic matter in the Jurassic of southern England and its relation to the burial history of the sediments. Journal of Petroleum Geology 93, 259–280.
Edgoose, C.J., 2012. The Amadeus Basin, central Australia. Episodes-News magazine of the International Union of Geological Sciences 35, 1–256.
Faber, E., Stahl, W., 1984. Geochemical surface exploration for hydrocarbons in North Sea. American Association of Petroleum Geologists Bulletin 68, 363–386.
Feng, S.N., 1991. New knowledge on Dongwu movement. Geoscience 5, 378–384 (in Chinese with English abstract).
Ficken, K.J., Li, B., Swain, D.L., Eglinton, G., 2000. An *n*-alkane proxy for the sedimentary input of submerged/floating freshwater aquatic macrophytes. Organic Geochemistry 31, 745–749.
Filby, R.H., 1994. Origin and nature of trace element species in crude oils, bitumens and kerogens: implications for correlation and other geochemical studies. Geological Society, London, Special Publications 78, 203–219.
Galarraga, F., Llamas, J.F., Martinez, A., Martinez, M., Flamas, J.F., Marquez, G., 2008. V/Ni ratio as a parameter in palaeoenvironmental characterization of nonmature medium-crude oils from several Latin American basins. Journal of Petroleum Science and Engineering 61, 9–14.
Galimov, E.M., 1985. The relation between formation conditions and variations in isotope composition of diamonds. Geochemistry International 22, 118–141.
Galimov, E.M., 1988. Sources and mechanisms of formation of gaseous hydrocarbons in sedimentary rocks. Chemical Geology 71, 77–95.
Guo, Z.W., Deng, K.L., Han, Y.H., Liu, Y.K., Yin, J.T., Wang, Q.G., Liang, E.Y., Li, G.J., Chen, Z.G., Liu, Z.Z., Wu, C.S., Zhao, Z.J., 1996. Forming and Evolution of Sichuan Basin. Geological Publishing House, Beijing, pp. 48–112 (in Chinese).
Gussow, W.C., 1968. Migration of reservoir fluids. Journal of Petroleum Technology 20, 353–365.
Hatch, J.R., Leventhal, J.S., 1992. Relationship between inferred redox potential of the depositional environment and geochemistry of the Upper Pennsylvanian (Missourian) Stark Shale Member of the Dennis Limestone, Wabaunsee County, Kansas, U.S.A. Chemical Geology 99, 65–82.
He, B., Xu, Y.G., Wang, Y.M., Xiao, L., 2005. Nature of the Dongwu Movement and its temporal and spatial evolution. Earth Science-Journal of China University of Geosciences 30, 89–96 (in Chinese with English abstract).
Hirner, A.V., 1987. Metals in crude oils, asphaltenes, bitumen and kerogen in Molasse Basin, Southern Germany. In: Filby, R.H., Branthaver, J.F. (Eds.), Metal Complexes in Fossil Fuels. American Chemical Society Symposium Series, vol. 344. Washington, DC, pp. 146–153.
Hoefs, J., 2008. Stable Isotope Geochemistry. Springer, Berlin.
Hou, F.H., Fang, S.X., Wang, X.Z., Huang, J.X., Li, L., Wang, A.P., Guo, L., Li, S.H., 1999. Further understandings of the gas-reservoir rocks of Sinian Dengying Formation in Sichuan, China. Acta Petrolei Sinica 20, 16–21 (in Chinese with English abstract).
Hu, S.Z., Fu, X.W., Wang, T.D., Li, T.J., 2007. Bitumen-sealed belt in reservoirs and its implication to petroleum exploration. Natural Gas Geoscience 18, 99–103 (in Chinese with English abstract).
Huang, J.Z., 2009. The pros and cons of paleohighs for hydrocarbon reservoiring: a case study of the Sichuan basin. Natural Gas Industry 29, 12–17 (in Chinese with English abstract).
Huang, J.Z., Chen, S.J., 1993. Geochemistry of source rocks for Sinian gas reservoir accumulation: Weiyuan gas field. Natural Gas Geoscience 4, 16–20 (in Chinese).
Huang, W.Y., Meinschein, W.G., 1979. Sterols as ecological indicators. Geochimica et Cosmochimica Acta 43, 739–745.
Huang, J.Z., Ran, L.H., 1989. Bitumen and oil-gas exploration in Sinian "Dengying Limestone" in Sichuan Basin. Acta Petrolei Sinica 10, 27–36 (in Chinese with English abstract).
Hunt, J.M., 1996. Petroleum Geology and Geochemistry. Freeman and Company, New York.
Jones, B., Manning, D.C., 1994. Comparison of geochemical indices used for the interpretation of palaeoredox conditions in ancient mudstones. Chemical Geology 111, 111–129.
Karlsen, D.A., Nyland, B., Flood, B., Ohm, S.E., Brekke, T., Olsen, S., Backer-Owe, K., 1995. Petroleum geochemistry of the Haltenbanken, Norwegian continental shelf. In: Cubitt, J.M., England, W.A., (Eds.), The Geochemistry of Reservoirs, Geological Society Special Publication No. 86. The Geological Society, London, pp. 203–256.
Karlsen, D.A., Skeie, J.E., 2006. Petroleum migration, faults and overpressure, part I: calibrating basin modelling using petroleum in traps—a review. Journal of Petroleum Geology 29, 227–256.
Klemme, H.D., Ulmishek, G.F., 1991. Effective petroleum source rocks of the world: stratigraphic distribution and controlling depositional factors. American Association of Petroleum Geologists Bulletin 75, 1809–1851.
Lerch, B., Karlsen, D.A., Matapour, Z., Seland, R., Backer-Owe, K., 2016. Organic geochemistry of Barents Sea petroleum: thermal maturity and alteration and mixing processes in oils and condensates. Journal of Petroleum Geology 39, 125–148.
Lewan, M.D., 1980. Geochemistry of Vanadium and Nickel in Organic Matter of Sedimentary Rocks Ph.D. Thesis. University of Cincinnati.

Lewan, M.D., 1984. Factors controlling the proportionality of vanadium to nickel in crude oils. Geochimica et Cosmochimica Acta 48, 2231–2238.
Li, J.Z., Dong, D.Z., Chen, G.S., Wang, S.Q., Cheng, K.M., 2009. Prospects and strategic position of shale gas resources in China. Natural Gas Industry 29, 11–16 (in Chinese with English abstract).
Li, J., Zhou, S.X., Gong, S.H., Zheng, Z.Y., Fu, D.L., 2013a. Biomarker characteristics of source rock and bitumen and oil-source correlation of paleo-reservoir in northeastern Sichuan. Lithologic Reservoirs 25, 54–62 (in Chinese with English abstract).
Li, J., Yu, B.S., Guo, F., 2013b. Depositional setting and tectonic background analysis on lower Cambrian black shales in the North of Guizhou Province. Acta Sedimentologica Sinica 31, 20–31 (in Chinese with English abstract).
Li, W., Yi, H.Y., Hu, W.S., Yang, G., Xiong, X., 2014a. Tectonic evolution of Caledonian paleohigh in the Sichuan Basin and its relationship with hydrocarbon accumulation. Natural Gas Industry 34, 8–15 (in Chinese with English abstract).
Li, W., Zhang, Z.J., Dang, L.R., 2011. Depositional systems and evolution of the Upper Carboniferous Huanglong Formation in the eastern Sichuan Basin. Petroleum Exploration and Development 38, 400–408 (in Chinese with English abstract).
Li, X.Q., Wang, Z.C., Zhang, W.X., Liu, Q., Yan, J.M., 2001. Characteristics of paleo-uplifts in Sichuan Basin and their control action on natural gases. Oil and Gas Geology 22, 347–351 (in Chinese with English abstract).
Li, Y.L., Wu, F.R., Liu, D.J., Peng, Y., Chen, S., Deng, X.J., Li, X.J., Gong, F.H., Chen, H., Gan, X.M., 2014b. Distribution rule and exploration prospect of the Longwangmiao Fm reservoirs in the Leshan-Longnvsi Paleouplift, Sichuan Basin. Natural Gas Industry 34, 61–66 (in Chinese with English abstract).
Li, Z.M., Gong, S.Y., Chen, J.Q., Su, W.B., 1997. Ordovician-Silurian depositional sequences and their relations with tectonic movement in South China. Earth Science-Journal of China University of Geoscience 22, 526–530 (in Chinese with English abstract).
Liang, D.G., Guo, T.L., Chen, J.P., Bian, L.Z., Zhao, Z., 2009. Some progresses on studies of hydrocarbon generation and accumulation in marine sedimentary regions, southern China (Part 2): geochemical characteristics of four suites of regional marine source rocks, South China. Marine Origin Petroleum Geology 14, 1–15 (in Chinese with English abstract).
Liu, B.J., Xu, X.S., 1994. Atlas of the Lithofacies and Palaeogeography of South China (Sinian-Triassic). Science Press, Beijing (in Chinese).
Liu, Q.Y., Jin, Z.J., Gao, B., Zhang, D.W., Xu, M.E., 2012. Types and hydrocarbon generation potential of the Permian source rocks in the Sichuan Basin. Oil and Gas Geology 33, 10–18 (in Chinese with English abstract).
López, L., Lo Mónaco, S., 2004. Geochemical implications of trace elements and sulfur in the saturate, aromatic and resin fractions of crude oil from the Mara and Mara Oeste fields, Venezuela. Fuel 83, 365–374.
López, L., Lo Mónaco, S., Richardson, M., 1998. Use of molecular parameters and trace elements in oil-oil correlation studies, Barinas sub-basin, Venezuela. Organic Geochemistry 29, 613–629.
Ma, W.X., Liu, S.G., Huang, W.M., Zhang, C.J., Xu, G.S., Yuan, H.F., 2012. Characteristics of Silurian Paleo-oil reservoirs and their significance for petroleum exploration on the southeast margin of Sichuan Basin. Oil and Gas Geology 33, 432–441 (in Chinese with English abstract).
Machel, H.G., Krouse, H.R., Sassen, R., 1995. Products and distinguishing criteria of bacterial and thermochemical sulfate reduction. Applied Geochemistry 10, 373–389.
Magoon, L.B., Dow, W.G., 1994. The petroleum system. In: Magoon, L.B., Dow, W.G. (Eds.), The Petroleum System-From Source to Trap: AAPG Memoir 60. American Association of Petroleum Geologists, Tulsa, pp. 261–283.
Mazeas, L., Budzinski, H., 2002. Molecular and stable carbon isotopic source identification of oil residues and oiled bird feathers sampled along the Atlantic coast of France after the Erika oil spill. Environmental Science and Technology 36, 130–137.
Moldowan, J.M., Seifert, W.K., Gallegos, E.J., 1985. Relationship between petroleum composition and depositional environment of petroleum source rocks. American Association of Petroleum Geologists Bulletin 69, 1255–1268.
Murray, A.P., Boreham, C.J., 1992. Organic Geochemistry in Petroleum Exploration. Australian Geological Survey Organization, Canberra.
Ni, Y.Y., Ma, Q.S., Ellis, G.S., Dai, J.X., Katz, B., Zhang, S.C., Tang, Y.C., 2011. Fundamental studies on kinetic isotope effect (KIE) of hydrogen isotope fractionation in natural gas systems. Geochimica et Cosmochimica Acta 75, 2696–2707.
Ohm, S.E., Karlsen, D.A., Phan, N.T., Strand, T., Iversen, G., 2012. Present Jurassic petroleum charge facing Paleozoic biodegraded oil: geochemical challenges and potential upsides, Embla field, North Sea. American Association of Petroleum Geologists Bulletin 96, 1523–1552.
Olsen, S.D., Filby, R.H., Brekke, T., Isaksen, G.H., 1995. Determination of trace elements in petroleum exploration samples by inductively coupled plasma mass spectrometry and instrumental neutron activation analysis. Analyst 120, 1379–1390.
Pedersen, J.H., Karlsen, D.A., Spjeldnæs, N., Backer-Owe, K., Lie, J.E., Brunstad, H., 2007. Lower Paleozoic petroleum from southern Scandinavia: implications to a Paleozoic petroleum system offshore southern Norway. American Association of Petroleum Geologists Bulletin 91, 1189–1212.
Peters, K.E., Walters, C.C., Moldowan, J.M., 2005. The Biomarker Guide, Biomarkers and Isotopes in the Petroleum Exploration and Earth History, vol. 2, second ed. Cambridge University Press, Cambridge, pp. 475–1155.
Quinby-Hunt, M.S., Wilde, P., 1996. Chemical depositional environments of calcic black shales. Economic Geology 91, 4–13.
Rayleigh, L., 1896. Theoretical considerations respecting the separation of gases by diffusion and similar processes. Philosophical Magazine Series 5 (42), 493–498.
Rooney, M.A., Claypool, G.E., Chung, H.M., 1995. Modeling thermogenic gas generation using carbon isotope ratios of natural gas hydrocarbons. Chemical Geology 126, 219–232.
Rylance, M., Nicolaysen, A., Ishteiwy, O., Judd, T., Huey, T., Giffin, W., 2011. Hydraulic fracturing: key to effective Khazzan-Makarem tight gas appraisal. In: SPE Middle East Unconventional Gas Conference and Exhibition 2011. Society of Petroleum Engineers, Muscat, Oman, pp. 476–490.
Sahu, H.S., Raab, M.J., Kohn, B.P., Gleadow, A.J.W., Bal, K.D., 2013. Thermal history of the Krishna-Godavari Basin, India: constraints from apatite fission track thermochronology and organic maturity data. Journal of Asian Earth Sciences 73, 1–20.
Schoell, M., 1983. Genetic characterization of natural gases. AAPG Bulletin 67, 2225–2238.
Schwark, L., Empt, P., 2006. Sterane biomarkers as indicators of Palaeozoic algal evolution and extinction events. Palaeogeography, Palaeoclimatology, Palaeoecology 240, 225–236.
Seifert, W.K., Moldowan, J.M., 1979. The effect of biodegradation on steranes and terpanes in crude oils. Geochimica et Cosmochimica Acta 43, 111–126.
Shen, J., 2014. The effect of the mineral compositions to shale gas of Longmaxi formation at Sichuan Basin Masters Thesis. Lanzhou University, pp. 1–40.
Shen, P., Zhao, Z.A., Zeng, Y.X., Yang, Y., 2007. Discovery of oolitic shoal reservoirs in Feixianguan Formation and the characteristics at northwest Sichuan. Journal of Southwest Petroleum University 29, 1–4 (in Chinese with English abstract).
Shi, C.H., Cao, J., Bao, J.P., Zhu, C.S., Jiang, X.C., Wu, M., 2015. Source characterization of highly mature pyrobitumens using trace and rare earth element geochemistry: Sinian-Paleozoic paleo-oil reservoirs in South China. Organic Geochemistry 83, 77–93.
Silverman, S.R., 1965. Migration and segregation of oil and gas. In: Young, A., Gally, J. E. (Eds.), Fluids in subsurface environments: AAPG Memoir 4. American Association of Petroleum Geologists, Tulsa, pp. 53–65.
Stahl, W.J., 1977. Carbon and nitrogen isotopes in hydrocarbon research and exploration. Chemical Geology 20, 121–149.
Sun, W., Liu, S.G., Wang, G.Z., Xu, G.S., Luo, Z.L., Han, K.Y., Yuan, H.F., Huang, W.M., 2010. Characteristics of gas formatted from Sinian to Lower Paleozoic in Weiyuan Area of Sichuan Basin, China. Journal of Chengdu University of Technology (Science & Technology Edition) 37, 481–489 (in Chinese with English abstract).
Swanson-Hysell, N.L., Maloof, A.C., Kirschvink, J.L., Evans, D.A., Halverson, G.P., Hurtgen, M.T., 2012. Constraints on Neoproterozoic paleogeography and Paleozoic orogenesis from paleomagnetic records of the Bitter Springs Formation, Amadeus Basin, central Australia. American Journal of Science 312, 817–884.
Tan, X.C., Luo, B., Cao, J., 2012. Gas accumulation in the Cambrian-Sinian of the Sichuan Basin Internal Technical Report. PetroChina Southwest Oil & Gas Field Company, Chengdu (in Chinese).
Tang, Y.C., Huang, Y.S., Ellis, G.S., Wang, Y., Kralert, P.G., Gillaizeau, B., Ma, Q.S., Hwang, R., 2005. A kinetic model for thermally induced hydrogen and carbon isotope fractionation of individual *n*-alkanes in crude oil. Geochimica et Cosmochimica Acta 69, 4505–4520.
Tang, Y.C., Perry, J.K., Jenden, P.D., Schoell, M., 2000. Mathematical modeling of stable carbon isotope ratios in natural gases. Geochimica et Cosmochimica Acta 64, 2673–2687.
Tenger, B., Qin, J., Fu, X., Yang, Y., Lu, L., 2014. Marine hydrocarbon source rocks of the Upper Permian Longtan Formation and their contribution to gas accumulation in the northeastern Sichuan Basin, southwest China. Marine and Petroleum Geology 57, 160–172.
Tissot, B.P., Welte, D.H., 1984. Petroleum Formation and Occurrence. Spring-Verlag, Berlin, Heidelberg, New York, pp. 339–374.
Tong, C.G., 2000. Relationship between neotectonic movement and structural evolution and gas pools formation of Sichuan Basin. Journal of Chengdu University of Technology 27, 123–130 (in Chinese with English abstract).
Volkman, J.K., Barrett, S.M., Blackburn, S.I., 1999. Eustigmatophyte microalgae are potential sources of C_{29} sterols, C_{22}–C_{28} *n*-alcohols and C_{28}–C_{32} *n*-alkyl diols in freshwater environments. Organic Geochemistry 30, 307–318.
Wang, D.F., 1995. A discussion on the tectonic zone of Middle Asia and its transformation to tectonic zone of circum Pacific Ocean in Eastern China. Journal of Geology and Mineral Research North China 10, 135–142 (in Chinese).
Wang, L.S., Zou, C.Y., Zheng, P., Chen, S.J., Zhang, Q., Xu, B., Li, H.W., 2009. Geochemical evidence of shale gas existed in the Lower Paleozoic Sichuan Basin. Natural Gas Industry 29, 59–62 (in Chinese with English abstract).
Wang, T.G., Han, K.Y., 2011. On meso-neoproterozoic primary petroleum resources. Acta Petrolei Sinica 32, 1–7 (in Chinese with English abstract).
Wang, Z.C., Jiang, H., Wang, T.S., Lu, W.H., Gu, Z.D., Xu, A.N., Yang, Y., Xu, Z.H., 2014. Paleo-geomorphology formed during Tongwan tectonization in Sichuan Basin and its significance for hydrocarbon accumulation. Petroleum Exploration and Development 41, 305–312 (in Chinese with English abstract).
Wei, G.Q., Liu, D.L., Zhang, L., Yang, W., Jin, H., Wu, S.X., Shen, J.H., 2005. The exploration region and natural gas accumulation in Sichuan Basin. Natural Gas Geoscience 16, 437–442 (in Chinese with English abstract).
Wei, G.Q., Shen, P., Yang, W., Zhang, J., Jiao, G.H., Xie, W.R., Xie, Z.Y., 2013. Formation conditions and exploration prospects of Sinian large gas fields, Sichuan Basin. Petroleum Exploration and Development 40, 129–138 (in Chinese with English abstract).

Wei, G.Q., Xie, Z.Y., Bai, G.L., Li, J., Wang, Z.H., Li, A.G., Li, Z.S., 2014. Organic geochemical characteristics and origin of natural gas in the Sinian – Lower Paleozoic reservoirs, Sichuan Basin. Natural Gas Industry 34, 44–49 (in Chinese with English abstract).

Wei, G.Q., Xie, Z.Y., Song, J.R., Yang, W., Wang, Z.H., Li, J., Wang, D.L., Li, Z.S., Xie, W.R., 2015. Features and origin of natural gas in the Sinian-Cambrian of central Sichuan paleo-uplift, Sichuan Basin, SW China. Petroleum Exploration and Development 42, 768–777.

Whiticar, M.J., 1996. Stable isotope geochemistry of coals, humic kerogens and related natural gases. International Journal of Coal Geology 32, 191–215.

Wilde, P., Lyons, T.W., Quinby-Hunt, M.S., 2004. Organic carbon proxies in black shales: molybdenum. Chemical Geology 206, 167–176.

Wu, W., Luo, B., Luo, W.J., Wang, W.Z., 2016. Further discussion about the origin of natural gas in the Sinian of central Sichuan paleo-uplift, Sichuan Basin, China. Natural Gas Geoscience 27, 1447–1453 (in Chinese with English abstract).

Xu, C.C., Li, J.L., Yao, Y.B., Yang, J.L., Gong, C.M., 2006. Cases of discovery and exploration of marine fields in China (Part 8): Triassic T_3j_2 reservoir of Moxi Gas Field in Sichuan Basin. Marine Origin Petroleum Geology 11, 54–61 (in Chinese with English abstract).

Xu, C.C., Shen, P., Yang, Y.M., Luo, B., Huang, J.Z., Jiang, X.F., Xie, J.R., Cen, Y.J., 2014. Accumulation conditions and enrichment patterns of natural gas in the Lower Cambrian Longwangmiao Formation reservoirs of the Leshan-Longnvsi Paleohigh, Sichuan Basin. Natural Gas Industry 34, 1–7 (in Chinese with English abstract).

Xu, H.L., Wei, G.Q., Jia, C.Z., Yang, W., Zhou, T.W., Xie, W.R., Li, C.X., Luo, B.W., 2012. Tectonic evolution of the Leshan-Longnüsi paleo-uplift and its control on gas accumulation in the Sinian strata, Sichuan Basin. Petroleum Exploration and Development 39, 406–416 (in Chinese with English abstract).

Xu, S.Q., Xiong, R.G., 1999. The forming, evolution of Caledonian paleouplift and its forming mechanism. Natural Gas Exploration and Development 22, 1–6 (in Chinese).

Xu, S.Q., Zhang, G.R., Li, G.H., Li, H.L., 2000. The hydrocarbon source condition of Sinian system of the Caledonian Palaeo-uplift. Journal of Chengdu University of Technology 27, 131–138 (in Chinese with English abstract).

Yan, D.T., Chen, D.Z., Wang, Q.C., Wang, J.G., 2009. Geochemical changes across the Ordovician-Silurian transition on the Yangtze Platform, South China. Science in China, Series D: Earth Sciences 52, 38–54.

Yang, Y., Zeng, Y.X., Liu, W., 2002. The control of Feixianguan Formation's sedimentary facies to oolitic beach reservoir in northeast Sichuan Basin. Natural Gas Exploration and Development 25, 1–9 (in Chinese).

Yao, G.S., Zhou, J.G., Zou, W.H., Zhang, J.Y., Pan, L.Y., Hao, Y., Wang, F., Gu, M.F., Dong, Y., Zheng, J.F., Ni, C., Xin, Y.G., 2013. Characteristics and distribution rule of lower Cambrian Longwangmiao grain beach in Sichuan Basin. Marine Origin Petroleum Geology 18, 1–8 (in Chinese with English abstract).

Zheng, J.F., Shen, A.J., Liu, Y.F., Chen, Y.Q., 2013. Main controlling factors and characteristics of Cambrian dolomite reservoirs related to evaporite in Tarim Basin. Acta Sedimentologica Sinica 31, 89–98 (in Chinese with English abstract).

Zheng, P., Shi, Y.H., Zou, C.Y., Kong, L.M., Wang, L.S., Liu, J.Z., 2014. Natural gas sources in the Dengying and Longwangmiao Fms in the Gaoshiti-Maoxi area, Sichuan Basin. Natural Gas Industry 34, 50–54 (in Chinese with English abstract).

Zhu, D.Y., Meng, Q.Q., Hu, W.X., Jin, Z.J., 2012. Deep Cambrian surface-karst dolomite reservoir and its alteration by later fluid in Tarim Basin. Geological Review 58, 691–701 (in Chinese with English abstract).

Zhu, G.Y., Zhang, S.C., Liang, Y.B., Ma, Y.S., Dai, J.X., Li, J., Zhou, G.Y., 2006. The characteristics of natural gas in Sichuan Basin and its sources. Earth Science Frontiers 13, 234–248 (in Chinese with English abstract).

Zhu, G.Y., Zhang, S.C., Liang, Y.B., Li, Q.R., 2007. The genesis of H_2S in the Weiyuan gas field, Sichuan Basin and its evidence. Chinese Science Bulletin 52, 1394–1404.

Zou, C.N., Du, J.H., Xu, C.C., Wang, Z.C., Zhang, B.M., Wei, G.Q., Wang, T.S., Yao, G.S., Deng, S.H., Liu, J.J., Zhou, H., Xu, A.N., Yang, Z., Jiang, H., Gu, Z.D., 2014a. Formation, distribution, resource potential and discovery of the Sinian-Cambrian Giant Gas Field, Sichuan Basin, SW China. Petroleum Exploration and Development 41, 278–293 (in Chinese with English abstract).

Zou, C.N., Wei, G.Q., Xu, C.C., Du, J.H., Xie, Z.Y., Wang, Z.C., Hou, L.H., Yang, C., Li, J., Yang, W., 2014b. Geochemistry of the Sinian-Cambrian gas system in the Sichuan Basin China. Organic Geochemistry 74, 13–21.

Zou, C.N., Yang, Z., Dai, J.X., Dong, D.Z., Zhang, B.M., Wang, Y.M., Deng, S.H., Huang, J. L., Liu, K.Y., Yang, C., Wei, G.Q., Pan, S.Q., 2015. The characteristics and significance of conventional and unconventional Sinian-Silurian gas systems in the Sichuan Basin, central China. Marine and Petroleum Geology 64, 386–402.